Optimization of Laser-Induced Breakdown Spectroscopy (LIBS) for application in the cork industry.

Hugo A. Veloso

Mestrado Integrado em Engenharia Física
Departamento de Física e Astronomia
2020

U. PORTO
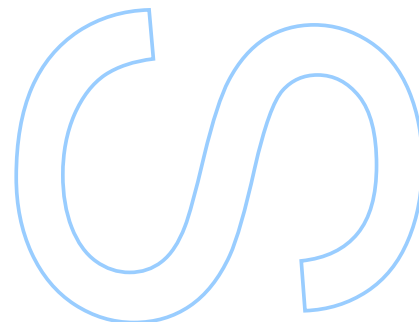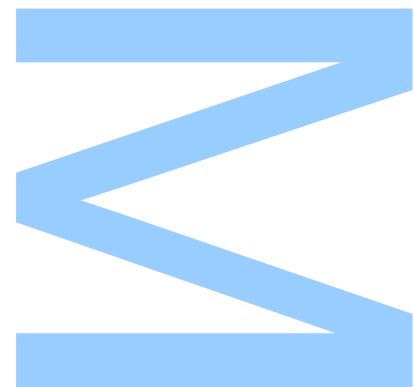
FACULDADE DE CIÊNCIAS
UNIVERSIDADE DO PORTO

Todas as correções determinadas

pelo júri, e só essas, foram efetuadas.

O Presidente do Júri,

Porto, _____/_____/_____

UNIVERSIDADE DO PORTO

MASTERS THESIS

Optimization of Laser-Induced Breakdown Spectroscopy (LIBS) for application in the cork industry.

Author:

Hugo A. VELOSO

Supervisor:

Prof. Dr. Pedro A. S. JORGE

Co-supervisor:

Dr. Diana GUIMARÃES

Dr. Rui MARTINS

A thesis submitted in fulfilment of the requirements

for the degree of MSc. Engineering Physics

at the

Faculdade de Ciências da Universidade do Porto

Departamento de Física e Astronomia

May 4, 2022

" The way a team plays as a whole determines its success. You may have the greatest bunch of individual stars in the world, but if they don't play together, the club won't be worth a dime. "

Babe Ruth

Acknowledgements

This past year has been tough for everyone, including me. Not only has the work done for this thesis consumed much of my time and energy, but a global pandemic has hit us hard, forcing us to confine ourselves, to change our habits and preventing us from leading a normal life. There have been ups and downs with this drastic change, but fortunately the people closest to me, both professionally and personally, have helped me through this most complicated phase. This way I would like to thank all the people who have helped me directly or indirectly in this final work. Starting with my supervisor, Dr. Pedro Jorge, and co-coordinators, Dr. Rui Martins and Dr. Diana Guimarães, who trusted me with an important project for them, I would like to thank you for the trust, help and knowledge that you have transmitted to me not only throughout the accomplishment of this work that I found interesting, but also in my integration in the team of the Center of Applied Photonics, where I was well received and could contribute and help the team, which I thank all the members for the support and good vibes of the workplace. A special thanks to Diana Capela for joining the Center of Applied Photonics team with me and for the help she has already given me since our entry into college.

Of course, there is no greater support in these times of greater work and stress as family. I want to thank my mother and sister, from the bottom of my heart, for motivating me and giving me inspiration and energy in the most monotonous and uncertain moments, both in the thesis and in my life. In the moments where the glass seemed half empty, they showed me that it was actually half full and pushed me to be better. Of course this course would not be the same without the presence and contribution of the friends I made during these years in college and that will be for life. From the evenings of study at the DCC to the gatherings at Casa do Povo, I learned a lot from them about being a good student , person and friend, them being always present for advice and help when needed.

Abstract

Faculdade de Ciências da Universidade do Porto

Departamento de Física e Astronomia

MSc. Engineering Physics

Optimization of Laser-Induced Breakdown Spectroscopy (LIBS) for application in the cork industry.

by Hugo A. Veloso

The invention of the Laser Source in the sixties proved to be an important step for modern science and for the development of new technologies that today are taken for granted. It opened many doors in the field of research, where new maximums of energy were possible to be reached and new processes created. One such process, developed by Debras -Guédon and Liodec, was the Laser Induced Breakdown Spectroscopy process, or LIBS, a spectroscopy process where laser pulses are sent and focus on a sample, vaporizing part of the sample and creating a weakly ionized plasma with the same chemical composition as the sample. With the decay of the plasma, the radiation emitted is captured and analysed. With this simple assembly process it is possible to carry out qualitative and quantitative analyses with a good degree of accuracy in the various desired scenarios, being a versatile method already integrated in several areas. In the context of the work developed here, the LIBS method has been studied for its application in cork stoppers, namely in the analysis of the quality of the protective coating of the cork stopper, with the aim of optimising the process for application in the cork stopper industry. Integrated in the team of the Center for Applied Photonics (CAP) at INESC TEC, the LIBS system developed by it was used, consisting of a 1064 nm Nd: YAG laser source with 8 ns of pulse width and adjustable energy through a Q-switch delay, an eight-channel spectrometer and a motorized stage. The intended analysis and studies were carried out using the Avasoft spectroscopy program and the Python 3.7 computational language. In order to find the ideal parameters for carrying out the analysis of the stopper coating, several analysis were made, starting with the observation of the influence of pulse energy in data

precision. The damage caused with several sets of laser shots and the influence of a lower energy shot before the main one were also analyzed. Shots with pulse energy of 20.9 mJ have been shown to generate the spectra with the highest precision and the least damage to the cork. In a final phase of study, maps of uniformity of the coating were prepared on stoppers with silicon and paraffin coating, in order to determine the feasibility of using the Principal Component Analysis method, a method of linear dimensional reduction, in the mapping of coating in scenarios where there is no characteristic line of the cork or coating. The PCA method proved to be viable for the elaboration of the uniformity maps, and it was possible to identify areas of absence of coating on the cork with this method as desired. In the future, and using these studies as base, the process could be improved in order to carry out more and other studies for its application in a future development of a LIBS prototype for stoppers.

UNIVERSIDADE DO PORTO

Resumo

Faculdade de Ciências da Universidade do Porto

Departamento de Física e Astronomia

Mestrado Integrado em Engenharia Física

Optimization of Laser-Induced Breakdown Spectroscopy (LIBS) for application in the cork industry.

por Hugo A. Veloso

A invenção da fonte laser nos anos sessenta provou ser um passo importante para a ciência moderna e para o desenvolvimento de novas tecnologias que hoje em dia são tidas como garantidas. Abriu muitas portas também no campo da investigação, onde era possível alcançar novos máximos de energia e criar novos processos. Um desses processos, desenvolvido por Debras-Guédon e Liodec, foi o processo Laser Induced Breakdown Spectroscopy, ou LIBS, um processo de espectroscopia em que os pulsos laser são disparados e focados numa amostra, vaporizando parte dela e criando um plasma fracamente ionizado com a mesma composição química que a amostra. Com a decomposição do plasma, a radiação emitida é capturada e analisadas. Com este processo de montagem simples é possível realizar análises qualitativas e quantitativas com um bom grau de precisão nos vários cenários desejados, sendo um método versátil já integrado em várias áreas. No contexto do trabalho aqui desenvolvido, o método LIBS foi estudado para a sua aplicação em rolhas de cortiça, nomeadamente na análise da qualidade do revestimento protector da rolha de cortiça, com o objectivo de optimizar o processo para a sua aplicação na indústria da cortiça. Integrado na equipa do Centro de Fotónica Aplicada do INESC TEC, foi utilizado o sistema LIBS por ela desenvolvido, constituído por uma fonte laser de 1064 nm Nd: YAG com 8 ns de largura de pulso e energia ajustável através de um Q-switch delay, um espectrómetro de oito canais e uma plataforma motorizada. As análises e estudos pretendidos foram realizados utilizando o programa de espectroscopia Avasoft e a linguagem computacional Python 3.7. A fim de encontrar os parâmetros ideais para realizar o estudo do revestimento da rolha, foram feitas várias análises, começando com

a análise da influência da energia de pulso na precisão dos dados. Foi também analisados danos causados com vários conjuntos de disparos de laser e a influência de um disparo de limpeza anterior ao pulso principal. Pulsos com energia de 20,9 mJ demonstraram gerar os espectros com a maior precisão e o menor dano à rolha. Numa fase final, foram preparados mapas de uniformidade do revestimento em rolhas com revestimento de silicone e parafina, a fim de determinar a viabilidade da utilização do método de Análise de Componentes Principais, um método de redução dimensional linear, no mapeamento do revestimento em cenários onde não existe uma linha característica da rolha ou do revestimento. O método PCA provou ser viável na elaboração dos mapas de uniformidade e na identificação de zonas de ausência de revestimento na rolha, conforme desejado. No futuro, e usando os estudos aqui feitos como base, o processo poderá ser melhorado a fim de realizar estudos mais precisos e novos para a aplicação destes num desenvolvimento futuro de um protótipo de LIBS para rolhas de cortiça.

Contents

xii

Optimization of Laser-Induced Breakdown Spectroscopy (LIBS) for
application in the cork industry.

List of Figures

xiv

Optimization of Laser-Induced Breakdown Spectroscopy (LIBS) for application in the cork industry.

xvi

Optimization of Laser-Induced Breakdown Spectroscopy (LIBS) for application in the cork industry.

Chapter 1

Introduction

In the 1960's, the invention of the *LASER* (*Light Amplification by Stimulated Emission of Radiation*) source changed the various fields of Science. Before its inception, the intensity of radiant energy that could be delivered was reaching its maximum potential due to the limitations of the technology at the time. *LASER* sources allowed the scientific community to achieve higher energies and intensities, turning some seemingly impossible experiments and applications into feasible projects. This made the laser source one of the most important discoveries of the XX century, heavily advancing our technology from there onwards. Nowadays, the *LASER* source is present in day-to-day lives. Even though it's already a versatile technology with multiple uses, such as sample analysis, data transmission, commercial purposes, industrial functions, and so on, it still has a lot of room to grow and improve.

One application made possible by the invention of the laser source is the ***Laser Induced-Breakdown Spectroscopy*** (**LIBS**), also known as ***Laser Induced-Plasma Spectroscopy*** (**LIPS**). Its history [1] [2] is closely connected to the history of the laser, beginning in 1962, where the idea of an analytical method to determine a sample composition was formed[2], involving plasmas created through laser pulses and collecting the emited light by the same plasma during its decaying process. A more detailed depiction of the LIBS method will be discussed in subsequent chapters.

The birth of the LIBS is associated to the work of *Debras-Guédon* and *Liodec* [2] made in 1963, where the first analytical use of spectrochemical analysis on surfaces was made. The setup consisted of a rubi laser of 100 J of energy and 100 μs of repitition rate being focused

1

2

OPTIMIZATION OF LASER-INDUCED BREAKDOWN SPECTROSCOPY (LIBS) FOR
APPLICATION IN THE CORK INDUSTRY.

in a 100 μm spot. With this instrument it was already listed the emission of 25 elements and detected molecular formation in the plasma. Quite a big start, don't you think?

In the period since its creation, LIBS has achieved many milestones. In the same year as of the work of *Debras-Guédon* and *Liodec*, LIBS plasma was created in gaseous and liquid samples[2] for the first time, making it theoretically possible to use LIBS in almost every material available. In the next year, *E. Archbold et al* produced the first time-resolved laser plasma spectroscopy[3]. By the 1980's , LIBS method was first analysed in aerosols, solid and molten metals, biologial materials, et cetera. Ironically, it was also in this decade that the acronym LIBS was first used. A portable version of LIBS was developed in 1992 with the purpose of monitoring surface contaminants, and by year 2000 LIBS was demonstrated on a NASA Mars Rover. A few years after, in 2012, LIBS was incorporated on the Mars Science Laboratory Rover. In the space industry, LIBS is used for characterization of, in these two last cases, the Mars' soil.

Motivation

Laser-Induced Breakdown Spectroscopy has shown a higher level of versatility compared to other methods of Atomic Emission Spectroscopy (**AES**). This versatility allows for different variations of the LIBS method to be built in order to optimize it for the intended purpose . Because LIBS uses the basis of atomic spectrochemical analysis, where a spectrum line is related to an atomic element, and is more affordable than other AES methods, it has entered in many research fields, industry sectors and can virtually be integrated in all areas where elemental analysis is needed. One of the areas where LIBS has not entered yet is the cork industry. Our team at the Center of Applied Photonics (CAP) at INESC TEC has an ongoing project with an engineering and industrial automation company in order to find a solution to improve cork characterization, namely in the evaluation of the uniformity and thickness of protective coatings present in cork stoppers. Being a microdestructive and versatile method, LIBS could be designed and developed for the evaluation of the cork stopper coating using sufficient parameters for a compact, specialized and affordable system.

Objectives

The main objective of this thesis is to explore the potential of LIBS for real time quality evaluation of cork stoppers for the cork industry. The existing methods of evaluation

of a stopper, although being of high precision, are expensive and destructive, turning the stopper unfit for use. LIBS is of simple construction and a micro-invasive method, possibly maintaining the integrity of the stopper. The idea is to determine the necessary configuration and parameter values of LIBS for a conclusive evaluation at a low cost and with low resource consumption. For that an existing LIBS prototype will be optimized for characterization of cork stoppers used in the cork industry and their protective coatings. This optimization study would involve energy studies, damage studies, uniformity map analysis and any other relevant study so as to optimize the instrument for successfull analysis while being cost efficient.

1.1 LIBS - State of the Art

To start the practical work of this thesis with a notion of the current state in which the LIBS technique is in, a search was made for scientific articles and projects where LIBS was used to study sample coatings and thin film samples. The objective was to have a clear notion of the capabilities of LIBS, the areas where it could be applied, some ideas that could be implemented in this thesis and also to make a comparative assessment between the different LIBS systems used so as to look for common configurations and parameters conventionaly used.

1.1.1 LIBS and Sample Coatings

Right of the bat many studies were found in multiple industries and areas that implement the same basis LIBS but in very different materials. An example is the characterization of vessel protective coating [4] and coating uniformity study for pharmaceutical tablets [14]. These and other papers will be covered below.

In 2000, C.C. Garcia *et al* developed a comparative study between LIBS and Laser-Ionization Time-oF-Flight Mass Spectrometry (LI-TFMS) for an in-depth characterization of a Zn-coated steel sample[4]. LI-TFMS uses a laser pulse for local ionization, where a mass analysis is made from the generated ions. Both LIBS and LI-TFMS are of rapid analysis and with negligable sample preparation. The two systems shared a 1064 nm, Nd:YAG laser source (Ultra CFR, Big Sky Laser Tech) with 6.5 ns pulse width and a laser radiation energy between 5 and 50 mJ/pulse. In the case of LIBS, the plasma light was carried throught a 0.5 m long quartz optic fiber cable of 540 nm core diameter. At the end the

plasma light was split by a 0.125 m Czerny-Turner Spectrograph (Oriel, MS125) and detected with a non-gateable CCD camera (Andor InstaSpec IV) with aquisition time of 17 ms. Measurements for depth profile analysis using LIBS and LI-TFMS were made in LI-TFMS vacuum and atmospheric pressure. Althought LI-TFMS showed reliable measurements with good resolution and repeatability in the depth profile analysis, vacuum-LIBS turned out to be a good alternative, giving a spectrum with low background, much narrower lines compared to atmospheric conditions and an absence of redeposited material. LIBS at atmospheric pressure provided more experimental flexibility in exchange for more data fluctuation compared to vacuum-LIBS and LI-TFMS.

The analysis of a titanium oxide coating using LIBS was done in 2008 by Hugo Estupiñán *et al*[5], with the intention of studying the feasibility of LIBS in the evaluation of titanium or Ti-alloy prosthesis coatings, in order to develop a faster, more effective and less costly method. From an unprepared titanium oxide film produced by anodization of a Ti_6Al_4V alloy, both thin film coating composition and plasma temperature were determined, the last by using Ti lines in the range between 470 and 520 nm using Boltzmann plot.

The LIBS system used by Estupiñán *et al* was comprised of a Q-switched Nd:YAG laser source with a laser pulse output of 532 nm wavelength and 10 ns pulse width, employing a 10 mJ pulse energy. Laser pulse was focused by a 100 mm focal distance quartz lens to create a plasma in a argon-filled chamber. The plasma emission radiation was focused by a 50 mm-focal length quartz lens and guided by an optical fiber to a spectrograph (Digikröm 740, Spectral Products) with 1200 grooves/mm diffraction grating, giving a resolution of 0.4 nm. The recording of the dispersed spectrum is done by a CCD detector (128H, Priceton Intruments), where the region between 760 and 790 nm was observed. The team behind the project concluded that LIBS can be used to determine the composition of thin films and to monitor and determine the uniformity of coatings.

LIBS method was also applied in the analysis of pharmaceutical tablet coating in regard to its uniformity in 2011 [6]. Atul Dubey *et al* underlines that the use of perforated coating pans, a popular method of applying coating in pharmaceutical tablets, has a well-known problem of suffering from slow axial mixing, causing a large variability in thickness and possibly making the pharmaceutical tablet unviable. Various methods for thickness evaluation have been used in this context , such as Near-Infrared (NIR) Spectroscopy, Terahertz Pulse Imaging and Raman Spectroscopy, but a rapid and inexpensive method to

assess intra and inter-tablet variability was needed for a quality-by-design approach in pharmaceutical manufacturing. With this in mind, a Pharmalaser Inc. commercial LIBS system was used, the PharmaLIBS^{TM} 250[7], which is composed by a Nd:YAG laser source operating at a fundamental wavelength of 1064 nm with pulse duration of 3-5 ns. Pulse energy was chosen to be 50 mJ, focusing on an area of 200 μm. The spectrograph of the system had a Czerny-Turner configuration with a spectral resolution of 0.1 nm. Nineteen locations in the tablets were ablated with 30 laser pulses in each location, and the Ti emission signal intensity, which represents the coating, was detected and recorded at 521.0 nm. The LIBS system developed was validated, allowing for a quick and efficient testing of large numbers of tablets in the final stage of production.

In 2012, Mateo *et al*[8] described the procedure used for a possible characterization of thickness and composition of the protective coatings applied in a vessel hull using LIBS. A depth analysis was made by firing consecutive laser pulses over a single position of the sample surface, where each shot is associated to a depth value relative to the sample surface. The evolution of the spectrum for each shot gives information about the composition and thickness of each layer of sample. The LIBS system used was a Q-Switch Nd:YAG laser source (Quantel, model Brilliant B) with laser pulse at the third harmonic of 355 nm and a FWHM pulse duration of 6 ns. This pulse delivered an energy of 104 mJ per pulse for depth profiling analysis in the multilayered sample, translating into a laser fluence of 8 $J\ cm^2$ over a sample area of 0.0132 cm^2. In order to maintain a constant crater diameter and fluence along the depth analysis, the depth of focus was set longer than the thickness of the sample. An Orial MS257 spectrometer with 0.08 nm of spectral resolution was used before the resulting splitted plasma light being registered by a Andor model DH 5H7-18D-03 ICCD (Intensified Charge Couple Device) detector with gate delay and gate width values of 500 ns.

The sample was a multilayered system of AH-36 grade structural steel covered in two layers of paint for protection of the bottom of the vessel: a green layer for corrosion prevention and a red layer for anti fouling. Initially, reference spectra for the green layer, red layer and steel substrate where recorded, showing a clear distiction between the three spectra that can be used in the depth profile analysis.

Depth of crater relative to each laser pulse fired was determined throught optical microscopy. Correlation depth profile was employed in depth analysis, where a mean value of 90 μm and 227 μm with a standard deviation of 11 μm and 12 μm, respectively, were

6

OPTIMIZATION OF LASER-INDUCED BREAKDOWN SPECTROSCOPY (LIBS) FOR
APPLICATION IN THE CORK INDUSTRY.

determined to the red and green layer, respectively. This article also showed the suitability of LIBS for quality control regarding depth profile analysis.

IN 2019, Basler *et al*[9] compared LIBS method for spatially resolved measurement of coating thickness between different laser pulse duration, namely for laser pulse durations of 290 fs, 10 ps and 6 ns. Five copper samples galvanized with a 5-30 μm thickness nickel coating were analysed. Consecutive laser shots were made in multiple locations of the sample and coating thickness was calculated by studying the spectrum evolution for Ni and Cu spectral lines. Comparison of these values with reference values obtained through XRF measurements were made.

To study LIBS with nano, pico and femtosecond laser pulses, two laser sources were used. The first was a Yb:YAG laser system (Light Conversion Carbide CB5-05) with a fundamental mode of 1028 nm wavelength and a tunable laser pulse width ranging from 290 fs to 10 ps. This laser source delivered 85 μJ per pulse with a maximum repetition rate of 60 kHz at full pulse power. The second laser source used was a Nd:YAG laser (Quantum Light Instruments, Q2-100) with 1064 nm wavelength pulse, with 6 ns pulse width and 250 μJ pulse energy. A polarizing beam splitter cube redirects the second beam through the same focusing lens to hit the same region as the first laser beam. For the collection of the plasma spectrum a Czerny-Turner spectrometer with a CCD-Line (Avantes Avaspec ULS2048L-EVO, Avantes BV) is used, with a 10 μm entrance slit, spectral resolution of 0.1 nm and integration time of 1.05 ms.

The team concluded that femtosecond pulse width returned the best results of coating thickness, followed not far behind by the picoseconds. Nanosecond pulse width showed the most inaccurate results between the three pulse widths. Ablation is one of the reasons for the difference in accuracy between pulse widths, since femtosecond and picosecond mostly ablates the material righ underneath the laser pulse when hitting the sample, while nanosecond pulses ablates the material below and immediatly around the focus point. LIBS in general showed itself to be a fast and accurate method with a promising role in the industry environment.

1.1.2 LIBS and Thin Film Samples

Thin films, i.e. materials tailored into thickness of range equal or below micrometer scale, is adopted in a variety of devices such as sensors , batteries, actuadors and other types

of technological devices [10]. For these devices the most important properties of the thin films are its chemical composition and structure, electrical, mechanical and optical characteristics. LIBS can be used in thin film samples for chemical composition and concentration.

J.D. Pedarnig *et al*[1] elaborated a project to study the characterization of nano-composite oxide ceramics using LIBS. With the same setup, monitoring of oxide thin film growth using LIBS was also tested in order to assess its viability. For this study, multi-component oxide ceramics and epitaxial thin films were analysed using a LIBS setup comprising a ND:YAG laser source with λ=1064 nm wavelength, pulse length of τ=6 ns and pulse repetition frequency of 20 Hz. The grated spectrometer used contained a CCD camera with recording range between 200 and 850 nm and spectral resolution of $\lambda/\Delta\lambda > 10\,000$. Delay time until recording was Δt_D=1 μm and gate width $\Delta t_G = 5$ μm. During thin film deposition, UV-excimer laser pulses with λ=248 nm, pulse width $\tau_L = 20$ ns and pulse frequency of 10 Hz in an oxygen rich environment were the conditions used. For characterization of the oxide ceramic samples, the data obtained came from twenty laser pulses for each of the six locations defined for each ceramic sample, making a total of 120 laser pulses per sample. The spectrum used for analysis corresponded to the average of the 120 recorded spectra. in the monitoring of thin film deposition, a spatially averaged spectrum was continuously recorded for more than ten minutes of deposition time during pulsed-laser deposition in HTS and ZnO ceramics. The results obtained point to the LIBS being a promising technique for in-line control of complex processes like multi-component material analysis and advanced material synthesis.

In 2015 Jung Hwan In et al [10] implemented a LIBS method for the evaluation of the composition of an unprepared $Cu(Inn, Ga)Se_2$ (CIGS) thin solar cell films, where an average composition of the film was predicted with less than 1% of relative standard deviation, corresponding to a high precision process. A commercial LIBS system (Applied Spectra Inc. RT250-EC) with a Nd:YAG laser source of 532 nm of wavelength, 5 ns of pulse width and top-hat profile was used for plasma formation, where a six channel CCD detector, with detection range between 187 to 1045 nm and 0.1 nm resolution, registered the emitted plasma radiation. This system was used for chemical composition identification and for depth profile analysis of the thin film samples, where reference values of composition and depth profile were taken by Inductively Coupled Plasma Optical Emission Spectroscopy (ICP-OES) and Secondary Ion Mass Spectrometry (SIMS), respectively. LIBS

8

OPTIMIZATION OF LASER-INDUCED BREAKDOWN SPECTROSCOPY (LIBS) FOR
APPLICATION IN THE CORK INDUSTRY.

predicted the four major elements In, Ga, Se and Cu from eight CIGS samples of different concentrations with a root mean square error in between $0.2 \sim 1.0\%$ range and a relative standard deviation (RSD) below 1.0% for all samples. For depth evaluation, depth profile from LIBS showed significant similarities with depth profile from SIMS, with depth resolution of less than 100 nm in a range between 0 and 2000 nm.

More recently in 2019, Hermann *et al*[11] had the aim of analysing multi-elemental thin films using Calibration-Free LIBS (CF-LIBS) as a complementary method or even replacing Rutherford Backscattering Spectrometry (RBS) or X-ray Photoelectron Spectrometry (XPS). In this study the team used a nickel-chromium-molybdenum alloy thin film of 150 nm of thickness produced by laser pulse deposition onto an electronic-grade low-resistivity Si(100) substrate of 99.999%. Coating thickness was deduced using RBS. The LIBS setup was equipped with a Nd:YAG laser pulse source of 266 nm of wavelength with laser pulse width equal to 4 ns and 6 mJ of energy per pulse. A 100 μm spot lead to a laser fluence of approximately 100 mJ cm^{-2} hiting the sample in an argon filled environment. An echelle spectrometer is used coupled with an ICCD detector. Values of delay time t_d and gate width t_g used followed the relation $\Delta t_d \leqslant t_d/2$. Measurements with multiple values of delay between laser pulse initiation and detector gate were made, where it was concluded that more accurate measurements were obtained using time interval from 1 to 2 μs of delay. Accuracy of the data obtained is depended on the uncertainty of the spectrometer, where the obtained 15% error margin can be reduced to 5% with accurate data.

Chapter 2

LIBS - Laser-Induced Breakdown Spectroscopy

2.1 Theory

2.1.1 Plasma and its formation

Just as the atoms and molecules of a substance in the liquid state have greater kinetic energy than they do in the solid state, and likewise in the gaseous state they present kinetic energy superior to the two previous states, the **plasma state** is the most energetic of the fundamental states of matter, being composed by molecules, atoms, ions and free electrons due to its high internal energy and kinetic energy. This mixture of electrons and ions, in aproximately equal number, leads to the neutral charge of the plasma at a macroscopic scale, where charged species interact collectively[12].

Plasmas can be characterized by a group of parameters, namely its temperature, degree of ionization and electron density. In regards to the degree of ionization, plasmas can be generally categorized into two groups[2]:

- **Weakly Ionized Plasma:** the ratio of electrons to other species is less than 10%;

- **Hightly Ionized Plasma:** the ratio of electrons compared to other species is very high.

10

OPTIMIZATION OF LASER-INDUCED BREAKDOWN SPECTROSCOPY (LIBS) FOR
APPLICATION IN THE CORK INDUSTRY.
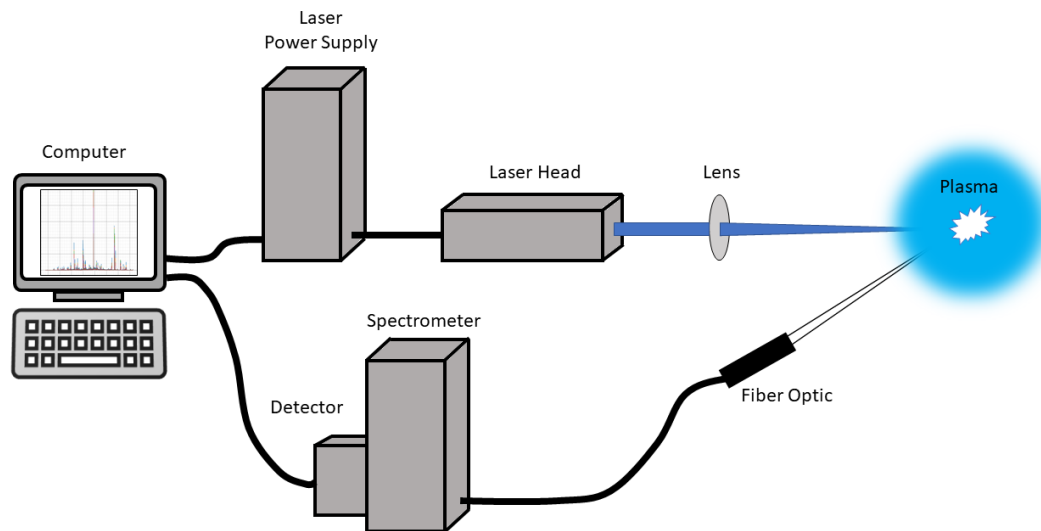
FIGURE 2.1: Simple representation of LIBS system (based on Figure 1.2 of [2])

2.1.2 Principle of LIBS

LIBS stands for *Laser-Induced Breakdown Spectroscopy*, an atomic spectroscopy method where the atomic composition of a sample is determined by looking at the spectrum emitted by a plasma created using laser pulses incident on the sample surface.

In a nutshell, LIBS can be divided into two phases. The firts phase is the LIBS plasma formation, where a laser pulse is focused on a small section of the sample of interest through the use of optical focusing lens. This incidence leads to the ablation of a small part of the sample. The remaining laser pulse energy ionizes the vaporized material and creates a weakly ionized plasma.

The second phase, i.e. the plasma radiation collection, [2] consists of the ions and electrons in the plasma experiencing recombination processes, consequently emitting an optical spectrum with well defined spectral lines characteristic of the atomic elements and/or molecules in the plasma. The light emitted by the plasma is then redirected throught the use of optical fibers, lenses and\or mirrors into a spectrometer or spectroscopic system, where the spectrum is recorded and analysed to determine the atomic composition of the sample. Figure 2.1 shows the representation of a basic setup of a LIBS system.

The total light spectrum emitted by the plasma is an overlap of the contribution of the background continuum and the ionic spectrum. As soon as the plasma is in its maximum ionization and plasma formation is interrupted, recombination and *bremsstrahlung* events
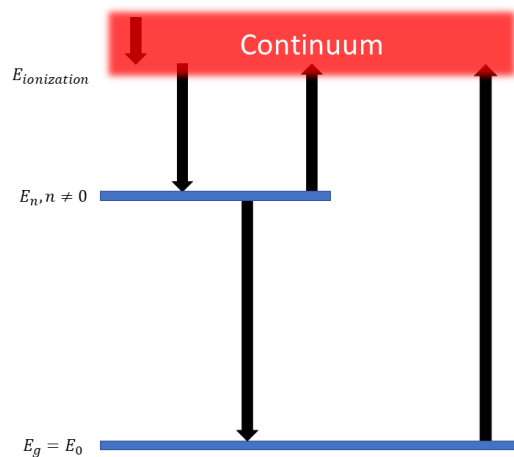
FIGURE 2.2: Possible transitions between electrons and atoms\ions. In the process or recombination, bound-bound and free-bound transitions are more relevant when it comes to the spectral lines detected. (based on Figure 1.2 of [2])
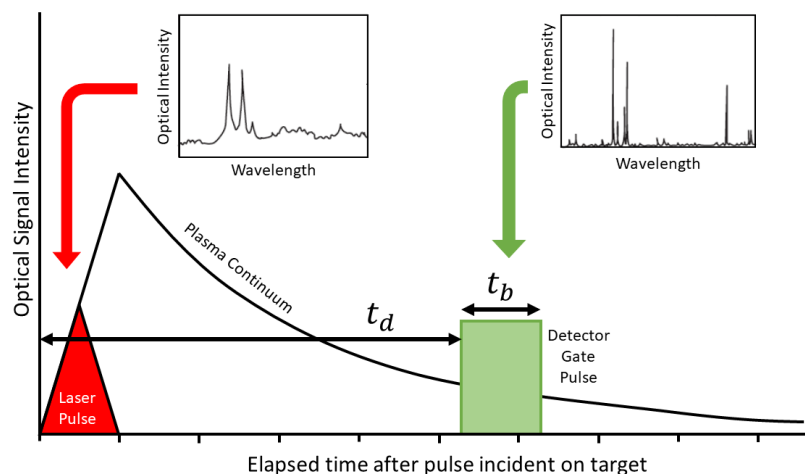
FIGURE 2.3: Schematic overview of the temporal evolution of a LIBS plasma (based on Figure 2.2 of [2]). Subplots above show examples of spectrum after laser initiation and at interval of t_d. In the latter, discrimination of spectrum lines is more evident.

occur, leading to plasma decay by radiation emission, with a rapid drop in plasma temperature. In recombination processes, a free electron is bonded into an ionic or atomic energy level, losing the excess of kinetic energy in the form of an emitted photon (free-bound). The *bremsstrahlung* process corresponds to the emission of photons by electrons decelerated by collisions with other free electrons in the continuum (free-free).

Due to recombination and bremsstrahlung processes, the background continuum decays faster than the spectral lines generated by spontaneous emissions within the atom

(bound-bound). Thanks to this phenomenon, one can choose the delay time between initiating laser and starting the record of the spectrum. With this, a good discrimination between the spectral lines and the background continuum can be obtained. An ilustration of the temporal evolution of a LIBS plasma can be seen in Figure 2.3, where t_d is the temporal delay between laser initiation and opening of recording window and t_b is the integration time.

The radiation emitted by the plasma depends on the atomic transitions occurring inside the plasma, where the transitions between levels with energy gap ΔE, in joules, are associated to the frequency, wavenumber and wavelength corresponding to, respectively [2]:

$$\nu = \frac{\Delta E}{h} \qquad \sigma = \frac{\nu}{c} \qquad \lambda = \frac{1}{\sigma} \tag{2.1}$$

For the LIBS process to be successful, the plasma generated from the sample must be an optically thin plasma, so that the self-absorption of radiation by the plasma is minimal and insignificant. If this condition is met, collision decay is more pronounced compared to radiative decay, thus causing the background continuum to decay faster than the emitted spectral lines of the plasma chemical elements, which are identical to those of the sample.

2.1.3   Spectral Lines

Thanks to the electron/atom transitions that occur during the decay of the plasma, photons with well-defined wavelengths will be emitted, leading to the appearance of spectral lines characteristic of the atomic matter in the plasma. These spectral lines have characteristics such as **width**, **profile shape** and **shift** that can provide information about some of the plasma properties like electron density, plasma temperature and broadening mechanism[2].

2.1.3.1   Spectral Profile and Broadening Mechanisms

Spectral line profile can give information about the broadening mechanism in the LIBS plasma. Some of the more common broadening mechanisms include natural broadening, Doppler broadening, collision (pressure) broadening, Stark broadening and Zeeman broadening [13]. Natural, Doppler and collision effects have been shown to give a higher contribution for line broadening[2].

Doppler broadening occurs when the emission of photons by a particle occurs while the particle is in motion. In this way, the frequency of the emitted radiation decreases as it
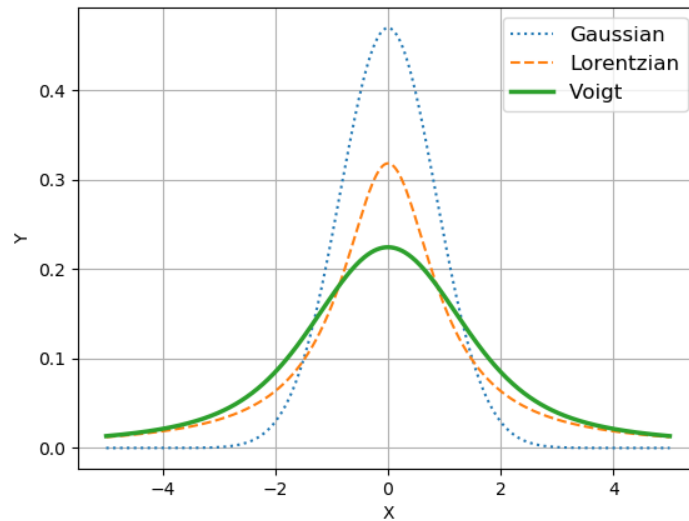
FIGURE 2.4: Voigt profile obtained by convoluting a Gaussian and Lorentzian profiles of same FWHM.

moves away from the emitting particle[14]. Pure Doppler broadening leads to a spectral line with **Gaussian profile**.

All excited quantum states have an intrinsic lifetime until they decay spontaneously into a lower energy state. **Natural line broadening** comes from the fact that a range of wavelengths can excite or deexcite the quantum transitions thanks to the Heisenber's uncertainty principle, which says that the uncertainty in the lifetime of the state, Δt, leads to an uncertainty in the energy state of a system, ΔE, following the relation $\Delta E \cdot \Delta t \geq \frac{h}{4\pi}$, where h is the Planck constant.

Collision broadening refers to the broadening influenced by collision with neutral atoms or molecules. Both natural and collision broadenings lead the spectral profile to a symmetric Lorentz profile[2].

During the plasma decay, Doppler, natural and collision broadenings occur with aproximately the same relative strength. Both Gaussian profile from Doppler broadening and Lorentz profile from natural and collision broadening will contribute for the final spectral profile, resulting from the convolution between the Gaussian and Lorentzian profiles. This convoluted profile is the **Voigt** profile. An example of a Voigt profile resulting from a Gaussian and Lorentzian profiles with same FWMH can be seen in Figure 2.4.

Collision broadening does not take into account collisions against ions and free electrons in the plasma. Instead, this type of collision leads to **Stark effect**. In this type of collision, the electric field of the charged particle (primarily with electrons) causes the

energy level of the atom to split into sub-levels. This causes the fine structure transition between sub-levels with differen t quantum number m_j to be asymmetric in relation to the unperturbed state[2]. The result of this can be a one-sided broadening of the peak width relative to the central wavelength, the so called **Stark broadening**, and/or a deviation of the peak from the expected central wavelength, depending on the intensity of the Stark effect.

Although not as common in LIBS plasma, the analogous effect of the Stark effect is the **Zeeman effect**. In this case, the splitting of the energy level into sub-levels is done by a weak magnetic field instead of an electric. This split due to the low magnetic field is symmetrical in relation to the unperturbed state. This effect also atributes a shift in the spectral line. If the magnetic field is strong, then comes in action the **Paschen–Back effect**, where a different pattern of splitting is caused by the strong magnetic field disrupting the coupling between orbital momentum m_l and spin angular momentum m_s [2][15].

2.1.3.2   Spectral Line Width and Electron Density

The level of ionization of the plasma can be determined by looking at the electron density. Estimation the electron density can be done from the width of the spectral line. The greatest contributions to line width are both **Doppler width** and **Stark effect**. Natural line width can be neglected since the Heisenberg uncertainty principle will cause the spectral width variation to be much less than the resolution of the spectrometers typically used in LIBS [2].

A usefull assumption generally made in LIBS is that the plasma is in Local Thermodynamical Equilibrium (**LTE**), where equilibration occurs in small regions of the plasma[2].This helps to estimate an accurate temperature of the plasma, from which various parameters can be calculated.

If LTE is observed, spectral line radiant intensity I, in W/sr, can be calculated from temperature in K using

$$I = \frac{hcN_o gA}{4\pi\lambda Z} exp\left(-\frac{E}{kT}\right) \tag{2.2}$$

where N is the total specie population, g the statistical weight of the state, A the Einstein coefficient , Z the partition function and E the energy of state, all associated to the desired line of wavelength λ. Parameters k,h and c are Boltzmann constant, Planck constant and speed of light, respectively.

This equation can also be used for graphical analysis to improve temperature values considering multiple spectral lines. Another way to estimate plasma temperature is by using the Two Lines method, where two spectral lines with known g,A,and E (statistical weights of the state, Einstein coefficient and energy of state, respectively) are used with Equation 2.2 to obtain

$$\frac{I'}{I} = \frac{\lambda g' A'}{\lambda' g A} \exp\left(\frac{-(E'-E)}{kT}\right) \tag{2.3}$$

To determine relative populations of energy level from temperature T and electronic density n_e, Boltzmann distribution is defined as

$$\frac{N_j}{N_i} = \frac{g_j}{g_i} \exp\left(\frac{-(E_j - E_i)}{kT}\right) \tag{2.4}$$

where $N_{i,j}$ are population of energy level i,j respectively and $g_{i,j}$ are the associated statistical weight of the levels with energy E_i and E_j, respectively.

Saha-Eggert equation can be used to determine temperature of ionization equilibrium if electron density n_e is known and relative intensities of lines from different ion stages of the same specie are measured. It can also be used the other way around to determine n_e. This is done using the following equation

$$\frac{N(Z,0)n_e}{N(Z-1,0)} = \frac{2(2\pi mkT)^{3/2}}{h^3} \cdot \frac{gA(Z,0)}{gA(Z-1,0)} \exp\left[-\frac{\Delta E}{kT}\right] \tag{2.5}$$

with $N(Z,0)$ being population of ground state of ionic stage Z and $N(Z-1,0)$ for ionic stage Z-1, and m the electronic mass.

2.1.4 Laser Ablation

With the incidence of the laser pulse on the sample, it undergoes ablation to a degree dependent on the properties of the material, the laser pulse, the surrounding environment and the interaction between the laser and the plasma.For ablation to be performed, a minimum power density value I_{min} must be exceeded for each laser pulse, this value being estimated, in units ofW/cm^2, from the Moenke-Blankenburg equation [2] defined as

$$I_{min} = \rho L_v \kappa^{1/2}/\Delta t^{1/2} \tag{2.6}$$
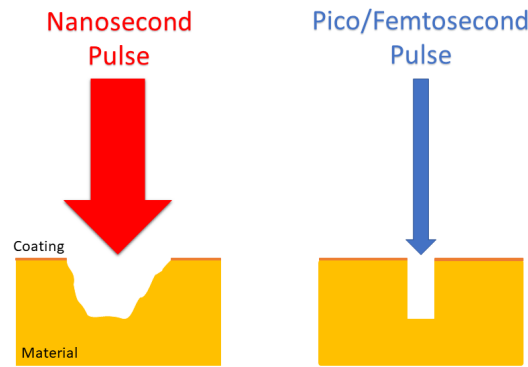
FIGURE 2.5: Results from interaction of different laser pulse widths with solid material
[2]. Holes made from pico or femtosecond laser pulse show a cleaner edge and precision,
due to the direct vaporization that occurs with short laser pulses.

where ρ is density of the material, L_v the latent heat of vaporization, κ the thermal diffusivity of the sample and Δt is laser pulse length. With this threshold exceeded, the maximum mass M of material that can be vaporized by the laser pulse can be determined by

$$M = E(1-R)/[C_p(T_b - T_0) + L_v] \tag{2.7}$$

where R is the surface reflectivity, C_p is the specific heat, T_b is the boiling point of the material in Kelvins, T_0 is the ambient temperature and L_v is the latent heat of vaporization. Depth ablation per pulse can be determined by substituting energy for fluence F and dividing by material density.

The behaviour of the pulse/material interaction is different depending on the width of the laser pulse. For micro and nanosecond laser pulses, the material undergoes heating, melting and vaporization during the incidence of the pulse, which leads to the appearance of wider and, for the nanosecond pulse, irregular holes. When using smaller width pulses, such as pico and femtosecond pulses, only direct vaporization occurs since absorption and interaction with the material occurs and finishes before plasma formation, thus not absorbing the laser pulse and creating a precise orifice. Figure 2.5 ilustrates the final result of interaction with the material using diferent pulse widths.

2.2   A brief talk about cork

Quercus suber L. is an evergreen oak commonly called cork oak. Cork oak forests occupy an estimated area of over 2.1 million hectares worldwide, mostly in the Western Mediterranean basin, with Portugal having 34% of the total area of cork forest, allowing it to be the largest producer of cork with 49.6% of cork production, being the cork stopper the most important cork-based product exported[16]. Cork oak, as the name suggests, is the primary source of cork, a 100% natural plant tissue that makes up the oak bark [17][16]. The macroscopic cellular structure of cork consists of hollow cells resembling a honeycomb, where the cell wall is made out of a primary wall of cellulose, a secondary wall of suberin and lignin, and a tertiary wall of polysaccharides[17]. These chemical compounds are made up of hydrogen, oxygen and carbon, in different chemical structures[16].

This material is used in several products, the best known being cork stoppers used in the bottling of alcoholic beverages such as wines, champagnes and others. There are several types of stoppers depending on their intended use and quality required. A protective layer is generaly placed inthe stopper during production in order to increase their resistance for a good removal when opening the bottle and for a good insulation of the liquid[16]. For these reasons the analysis of the homogeneity and thickness of the coating with a high degree of accuracy is of high importance. In this context, LIBS appears to be a good candidate for a micro-invasive analysis of the thickness and uniformity of the coating of cork stoppers. In this way the work here present will aim at the optimization of this method for its use in the cork stoppers industry for quality control of the protective coatings.

Chapter 3

Experimental Methods

Currently, cork stoppers are assesed by sampling and tensile testing to evaluate the quality of its coating. This approach is destructive, so the cork is unfeasible for use after the analysis. In order to fill the need for a micro or non-destructive method in the evaluation of stoppers, LIBS was considered since it is a rising micro-invasive process used for multielemental analysis in real time and with the capability to perform depth profile analysis and thin films deposition thickness control. These kind of analysis and studies using LIBS were already carried out in several areas of expertise, as indicated in the state of the art. Thus, LIBS can be easily modified to use in the context of the cork stoppers using the known LIBS theory, the knowledge acquired in the articles mentioned in the state of the art and adapting it to the reality of the cork industry.

The main objective of this work is to study and optimize LIBS analysis for measuring and evaluating of the protective coating of cork stoppers. With this, it is possible to create the basis for a future prototype of specialized LIBS system for stoppers that is of low cost and good accuracy. The distinction between types of stoppers and coatings was also studied, so that the future prototype could indicate the materials of the analyzed stopper and coating and set the ideal parameter values for that stopper/coating combination.

3.1 Equipment Used and Data Processing

3.1.1 LIBS Setup used

For this work, the LIBS system used was the already existing system (Figure 3.1 belonging to the team of the Center for Applied Photonics at INESC TEC, based on the Faculty of Sciences of the University of Porto. It is equiped with a 1064 nm, Q-switched Nd:YAG
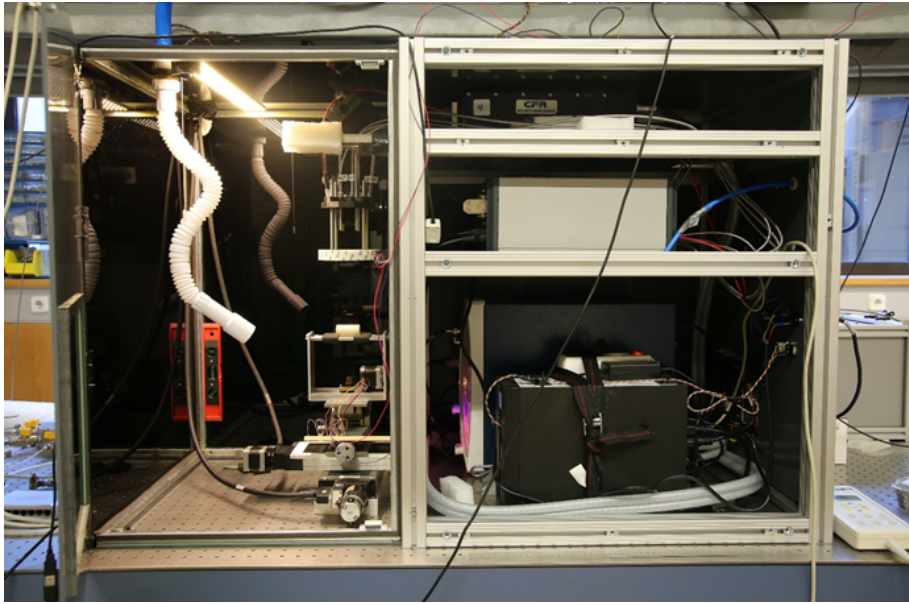
FIGURE 3.1: Experimental setup of the team.

laser source which emits laser pulses with 8 ns of pulse width and variable energy up to 211 mJ per pulse. Laser pulse is focused through a lens with focal distance of 20 cm in order to hit the sample, in this case the cork stoppers. The cork stoppers are put on a sample holder, 3D printed to accomodate corks, placed on top of a stage where xy-axis are motorized and height of the sample holder is manually controlled. The position of the sample along xy-axis was controlled directly by a *Newport Universal Motion Controller* (Model ESP7000) or by sending the desired coordinates through a COM link with the laboratory computer using a Python script developed specifically for this purpose.

The plasma emission light is collected by a set of eight optical fibers and redirected into a 8-channel, high resolution spectrometer (AVANTES AVS-Rackmount-USB2), with 16348 pixels, a wavelength detection range between 178 and 927 nm and resolution between 0.01 and 0.12 nm, depending on the channel in question (Table 3.1). Each channel separates the associated wavelength range from the rest of the spectrum, that portion

Channel	Range (nm)	Resolution (nm)
1	178 - 255	0.03 - 0.05
2	251 - 316	0.02 - 0.04
3	310 - 364	0.01 - 0.04
4	360 - 402	0.01 - 0.03
5	400 - 494	0.03 - 0.06
6	493 - 626	0.04 - 0.08
7	620- 727	0.03 - 0.07
8	725 - 927	0.07 - 0.12

TABLE 3.1: Determined resolution of each channel of the AVANTES spectrometer used.

being recorded by a CCD. The CCD con-
verts the optical signal into an electrical
signal, which is sent to the computer to perform the desired analyses. The integration
delay and integration time can be varied, with the minimum possible integration time
being 1.3 μs for integration delay and 1.05 ms for integration time.

3.1.2   Data Aquisition and Manipulation

The laser pulse firing and acquisition process was controlled by computer using the Py-
thon 3.7.4 computational language and the AvaSoft 8 spectroscopy program, respectively.
Using Python scripts previously developed by the team, new scripts were developed to
send the information of the necessary parameters to the controller of the carriages and
to the laser system, in order to carry out the desired laser shots in the intended locations
of the sample. The parameters sent are: Q-switch delay, associated with the laser pulse
energy, the relative coordinates of the points in the sample where the shots are to be fired,
and the number of consecutive shots desired in the same coordinate. Parameters such as
integration delay and integration time, which are associated with the spectrometer, are
defined beforehand in the spectroscopy program AvaSoft 8, which controls the operation
of the spectrometer. The detected spectra are then sent and saved on the computer for
data processing and further analysis.

   Using developed Python scripts, the recorded data are then organized in descending
hierarchical order Nodes, Shots and Channels, in order to be able to both select all the
spectra recorded in a spot (node) as well as one shot or only one channel of one shot. This
way, only the data desired for the analysis is accessed, thus reducing the execution time
and saving computational memory.

   After the organization has been completed, the spectra undergoes corrections in order
to remove the influence of the background continuum. This process is discussed in more
detail later, together with the collection of the intensity associated with a wavelength and
the detection of spectral peaks.

3.1.2.1   Baseline Correction

Once the information of the spectra made from a set of measurements is acquired, data
treatment is performed before its analysis, where the background contribution is removed.
As already mentioned, the collected spectrum is composed by a combination of the ionic

spectrum, background spectrum and the influence of dark current. The last two are not relevant for the analysis, and it is intended to remove their influence from the spectrum and, ideally, maintain the ionic spectrum. Contribution from the dark current can be overlooked since its order of magnitude is much smaller compared to the other two.

An algorithm was used to calculate an estimate of the background along the wavelength range and remove it from the spectrum initially recorded, namely the Asymmetric Least Squares Smoothing (ALS), developed by Paul Eilers and Hans Boelens [18][19] [20]. This algorithm uses Whittaker smoother defined as

$$S = \sum_i w_i \left(y_i - z_i\right)^2 + \lambda \sum_i \left(\Delta^2 z_i\right)^2 \quad (3.1)$$

where S measures the fit to the data, y is the signal, z is a smooth series and w is a weight vector. The first term of S represents the fit of the data while the second term is a penalty on non-smooth behavior of z, where λ, being a tuning parameter between both terms, sets the weight of the second term for a soft or hard smoothing of z. Large value of λ leads to a smoother z. Simplifying Equation 3.1 leads to

FIGURE 3.2: Flowchart of the ALS process implemented in Python, giving the recommended values of p and λ equal to 0.01 and 10^5 and a number of interations of $n_{inter} = 10$.

$$\left(W + \lambda D^{-1}D\right)z = Wy \qquad (3.2)$$

with $W = diag(w)$ and D is difference matrix $Dz = \Delta^2 z$. A weak smoothing can remove noise from the data, while a strong smoothing returns the slowly varying trend of the signal[18]. The choice of asymmetric weight follows the conditions

$$w_i = \begin{cases} p, & \text{if } y_i > z_i \\ 1 - p, & \text{if } y_i \leqslant z_i \end{cases} \qquad (3.3)$$

where p is an asymmetric parameter recommended to be set between 0.001 and 0.1. Giving λ and p, a smoothed baseline is updated interatively. Since z is the solution to equation 3.2,weight vector w is given as an array of ones. For each iteration w is updated , where the equation is solved again and z is updated. This process ends when w is shown to be constant after a certain number of iterations or when all the iterations are performed. Recommended values for p, λ and number of iterations, n_{iter}, were in the ranges $[0.001; 0.1]$, $\left[10^2; 10^9\right]$ and $[5; 10]$, respectively. The values chosen were $p = 0.01$, $\lambda = 10^5$ and $n_{iter} = 10$. A flowchart of the ALS algorithm is represented in Figure 3.2.

24

OPTIMIZATION OF LASER-INDUCED BREAKDOWN SPECTROSCOPY (LIBS) FOR
APPLICATION IN THE CORK INDUSTRY.
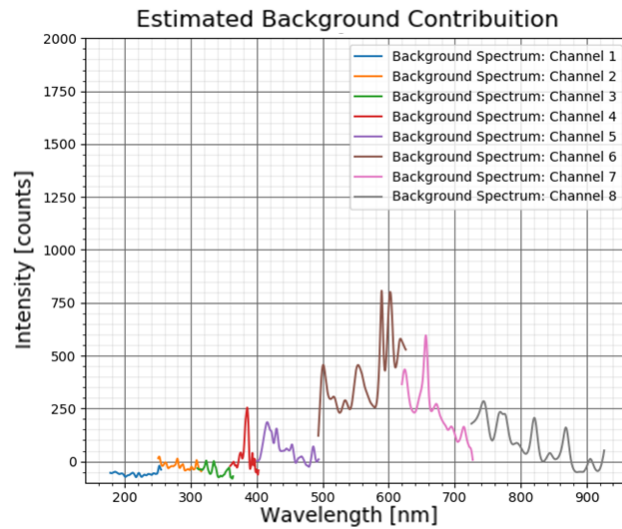
(A) Estimated background continuum for each of the channels using ALS.
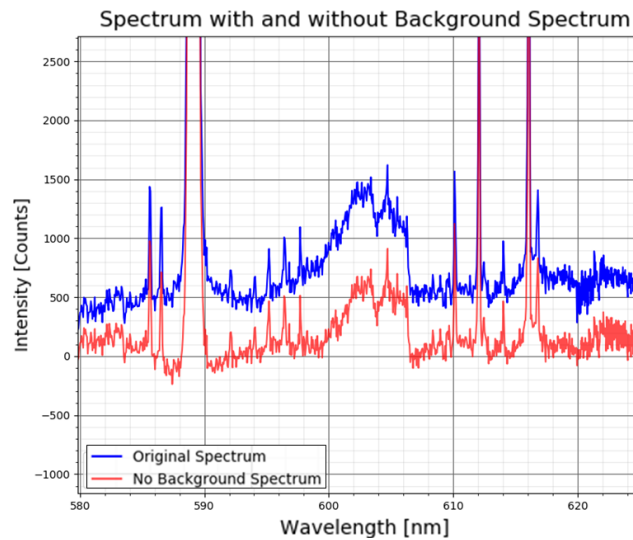
(B) Wavelength range where correction is more noticable.

FIGURE 3.3: Estimation of background continuum of spectrum recorded with the first laser pulse of 63 mJ of pulse energy on a Si-coated cork stopper (A). This estimation is removed from the spectrum for a more accurate reading. (B) is an interval of the spectrum were background continuum removal is more noticeable.

Figure 3.3 (A) shows an example of the estimated background spectrum for each channel of the spectrum. Figure 3.3 (B) shows, for the same example, a wavelength interval where it is more noticeable the disparity between the original spectrum recorded and the resultant spectrum when removing the estimated background in (A). This estimation of baseline correction is done individually for each spectrum recorded. More details abouts ALS are presented in [18],[19] and [20].

3.1.2.2 Limit of Detection

Limit of detection (LOD) is the lowest amount of the analyte of interest that can be distinguished with a specific degree of certainty. Below this threshold there is a greater uncertainty on the measurement due to the proximity to the background noise. As mentioned above in the previous subsection about background contribution, the total recorded spectrum contains the influence of the background and the dark current. Once the background spectrum has already been removed, ideally only noise and small fluctuations in intensity remain in the spectrum along with the detected spectral peaks. Thus, a DL spectrum was created from the recorded spectrum where the spectral peaks were removed, in order to more accurately estimate the mean and standard deviation of the noise of the registered spectrum. Thus LOD can be calculated using

$$y_L = \bar{y} + k\sigma \tag{3.4}$$

where $\bar{y}$ is the mean value of noise with standard deviation σ and k is the numerical factor associated to a confidence level, conventionally chosen to be 3 as to return a confidence level of 99.73% . For the estimation of the DL spectrum without the spectral peaks the Z-score parameter was considered[21]. Z-score gives information about how far a value is from its mean in standard deviation units

$$z_i = \frac{y_i - \bar{y}}{\sigma} \tag{3.5}$$

Spectral intensities with z-scores above a conventional value of 3 are considered peaks, these being disregarded, removed from the spectrum and substituted by an average value between its neighboring spectral intensities.

Unfortunately, since the intensity of the larger peaks is much higher than the noise values, the result of the average intensity was shown to be inflated and, consequently, smaller peaks were forgotten with this approach. The solution used involved the use of a modified Z-score parameter [21] that uses the value of median and median absolute deviation (MAD) in place of the mean and standard deviation, respectively. In this way, there is no inflation of the benchmark value.

$$z_i = 0.6745 \cdot \frac{x_i - M}{MAD} \tag{3.6}$$

26

OPTIMIZATION OF LASER-INDUCED BREAKDOWN SPECTROSCOPY (LIBS) FOR
APPLICATION IN THE CORK INDUSTRY.
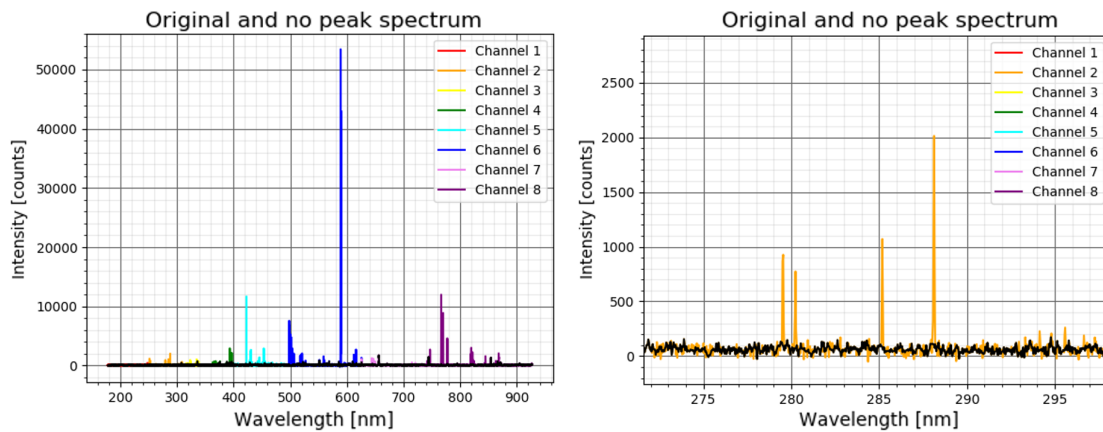
FIGURE 3.4: Example of estimated spectrum signal without peaks for the calculation of median and median absolute deviation used by the modified Z-score (left). This will lead to the calculation of the Limit of Detection. In the right, it can be seen that peaks of Si were successfully removed for the spectrum.

with M being the median value and $MAD = median\left(|x - M|\right)$. The constant 0.6745 corresponds to the 0.75th quartile of the standard normal distribution, to which MAD converges to.

With this the wavelengths of the spectrum that have a spectral peak are identified. Then m neighboring wavelenghts, also with no peaks, are used to average a value of noise intensity in that region. The final result is a similar spectrum to the original without the spectral peaks. That way a good estimation of average noise intensity and standard deviation can be made and a reliable LOD can be calculated using equation 3.4. Note that this process is done for each of the eight parts of the spectrum associated with the respective channel of the spectrometer that registered it, where each part of the spectrum has a corresponding LOD value. An example of the estimated spectrum with no peaks is presented in Figure 3.4.

3.1.2.3 Intensity Determination.

With the background spectrum removed and the LOD determination being possible, obtaining the intensity of a wavelength is the next step, a step that all subsequent algorithms will depend on.

To determine the intensity value of the wavelength in question, an LOD is previously calculated for the channel of the spectrometer the wavelength is in. The input data of the algorithm is the values of wavelength and intensity recorded by that channel, the

wavelength to be used, the determined LOD and the distance from the center of the peak which is to be used to search for the peak closest to the desired value. This interval value was defined as 0.10, that is, the intensity of a peak λ will be searched for in an interval [λ -0.10; λ + 0.10].

In a second step, local maximums are determined using the Python function *scipy.argrelextrema* and by looking at the slope with the next wavelength. Initialy the script considers a intensity y_i, from the local maxima determined by *scipy*, as a peak if one of the following four conditions is met:

1. angle of slope between y_i and y_{i+1} is similar to slope of y_{i-1} with y_i

2. intensity y_{i-1} is equal to y_{i+1};

3. if $y_{i-1} > y_{i+1}$, then y_i is considered to be $y_i = y_{i-1} + (y_i - y_{i-1})/2$, with $x_i = x_{i-1} + (x_i - x_{i-1})/2$

4. if $y_{i-1} < y_{i+1}$, then y_i is considered to be $y_i = y_i + (y_{i+1} - y_i)/2$, with $x_i = x_i + (x_{i+1} - x_i)/2$

These conditions correspond, respectively, to the following particular cases:

1. If slope between points adjacent to the local maxima determined by *scipy* are very similar;

2. If the intensity of the points adjacent to the maximum location detected is equal;

3. If 2) is not satisfied, a midpoint between the determined maximum and the nearest adjacent is considered. This the same for previous point 4)

Once the points that satisfy one of the above conditions have been saved, the wavelength of the data is searched for within the search limit that is provided, in this case related to the resolution of the spectrometer where the wavelength is present. If this experimental wavelength exists in the data, it is returned if its intensity value is higher than the calculated Limit of Detection. Otherwise it is considered to be spectral noise.

3.1.2.4 Peak Element Search

A Python script was also developed that searches for peaks of a desired element. This search uses the reference values present in the NIST database [22] for atomic emission lines.

Using the script mentioned in the previous subsection, the wavelength of the peaks present in the recorded spectrum is determined. These are compared with the wavelengths of the NIST database for the desired element, and this wavelength and its experimental intensity are saved if the separation between both wavelengths is lower than the resolution value of the spectrometer channel where the experimental wavelength was detected.

The script then compares the ratio between the experimental peaks and the ratio of the NIST peaks for the same element, where the peaks with very different ratios from the database are discarded. Although still prone to errors, it is possible to identify multiple emission lines characteristic of the elements, including the four characteristic Si peaks that were used for energy study and uniformity map generation, as will be discussed in Chapter 4.

3.1.2.5 PCA - Principal Component Analysis

One of the main objectives of this thesis was to discriminate the different types of stoppers and their coatings, when present. To perform a reliable comparison between spectra, it's necessary to check for differences in the pattern of the spectra. Performing this comparison for each wavelength value is both time consuming and has a high computational memory comsumption. In this way, it would be ideal to reduce the number of dimensions of the data down to the most relevant dimensions so as to allow for a simpler analysis without significant loss of information. With this in mind, the **Principal Component Analysis** algorithm, or **PCA**, was chosen as the solution for reducing data size.

Principal Component Analysis [23] is a multivariate statistical technique generally used with the intention of performing a data reduction while the relevant information is maintained. Briefly, PCA estimates a correlation structure of the variables and searches for the orthogonal directions of greatest dispersion of the data. These orthogonal directions are the *principal components*. A more understandable dimensional representation without much loss of information can be made using a vector space with the most relevant principal components as eigenvectors of said space. Patterns, clusters and outliers, not visible at first sight, can be identified using PCA.

A standardization of the data set is advised before initiating PCA since the method is sensitive to variances of variables with larger range behavior. Standardization of the data is made using the mean and variance values, using again the *Z-score* defined by the

equation 3.5 .This allows for the variables with greater range of variation not to dominate over variables with a smaller range.

An adequate explanation of the mathematical process of the PCA method can be read in the article written by Jonathon Shlens [24].

The implementation of the PCA method in Python was done as follows:

1. For each set of measurements, a dataframe is created where each column corresponds to a recorded wavelength, each line corresponds to a spectrum and cells are the intensity value of the associated wavelength and spectrum. A desired characteristic can be associated to each spectrum in order to be color coded and more easily identified on the final plot.

2. Standardization of the dataframe values is made using *StandardScaler().fit_transform* function from the *scikit-learn* package. This function removes the average value from the data values and resizes them in units of variance,i.e., it converts data values into the respective Z-score values.

3. After the standardization, the function *sklearn.decomposition.PCA* is used to determine the two most relevants principal component, where it executes linear dimensionality reduction using Singular Value Decomposition of the data to project it to the lower dimensional space desired[25].

From this process, we obtain the set of PC1 and PC2 values for each measurement, which are the principal components with the first and second most variance, respectively. This means that, for the same displacement in in both principal components, PC1 displacement has more impact in the data compared to PC2 and so on.

Chapter 4

Studies and Analysis

Moving on to the laboratory work of this thesis, several studies were developed and carried out in order to develop a more specialized LIBS method for its application in the cork stopper industry, namely in the evaluation of cork stopper coating. The following subsections will describe the labotatory studies, the results obtained and the data and interpretation made using Python scripts developed for the intended purpose. After carrying out these initial studies, the most relevant study of this work was executed, i.e., the mapping of the uniformity of a cork stopper coating.

These studies can also be used as a first step for the development of a prototype LIBS system specifically engineered for cork stopper analysis. Studies such as influence of laser pulses in the damage made, energy pulse variation for signal optimization and influence of a prior clean shot were made prior to the uniformity analysis.

4.1   Energy study and representative lines selection

To optimize the LIBS performance for the analysis of stoppers, a study of the influence of pulse energy on the quality of the spectral signal acquired was devised. For this study, consecutive shots were made at different points of the cork with different pulse energy values. The spectral signal was recorded and the Relative Standard Deviation, RSD, defined as ratio between the standard deviation and the average value, of the intensity of the lines of interest were determined. This was made due to the reciprocal relation between RSD and Signal-to-Noise ratio, S/N [26]. In the case of stoppers with silicon coating, the RSD was performed using the lines associated with the element.

In a first set of measurements made, for each value of Q-switch delay used, two consecutive laser pulses were fired in eighty spots. The Q-swich delay parameters used were 390, 380, 370, 360, 350 and 340 μs, which correspond to energy values of 15.1, 20.9, 27.9, 35.0, 41.6 and 48.3 mJ, respectively. With the collected spectra from the total of 960 laser pulses fired, the average intensity count, standard deviation and RSD of the main Si peaks detected were calculated, so as to determine the energy that leads to more accurate results.

FIGURE 4.1: Relative intensities of Si lines detected, relatively to peak at 288.13, according to the database of NIST.

From the possible Si peaks that were detected, the ones used for the calculations were those present in at least 80% of the spectra, so as to rule out all falsely detected peaks and to use a small but relevant group of lines that accurately represent the Si element. This reduced the number of peaks considered down to 10, which was found to be sufficient for analysis. Figure 4.1 shows the reference values of relative intensity, from the NIST database, for the detected Si lines relative to the peak at 288.16 nm, peak already know as being characteristic of silicon. By looking at the ratio of spectral peak intensities, it is possible to observe whether the ratios of the experimental peaks coincide with the reference ratios, thus proving, with a greater degree of certainty, that the lines are characteristic of Si. The Si peaks wavelength had a small shitf in their value by the hundredths, which can be attributed to resolution of the spectrometer. As an example, the 288.16 nm peak of Si was found at 288.13 nm in all spectra, which is a shift of 0.03 nm well inside the resolution of the spectrometer.

Figures A.4 and A.5 in Annex represent the average intensity in counts and associated standard deviation, respectively, for a given spectral line at a certain pulse energy value. Figure 4.2 (A) shows the relative intensity of the detected peaks of Si compared to the peak at 288.13 nm, the most intense of the peaks identified, while Figure 4.2 (B) is the associated RSD values of the same detected peaks.

Comparing the relative intensity of the experimental peaks and the reference peaks, the peak at 252.40, 323.36, 431.38 and 455.24 nm were discarted from analysis since their experimental values of relative intensity showed a large shift in relation to the reference values (Figure 4.1). It should be noted that the peaks considered viable were defined as
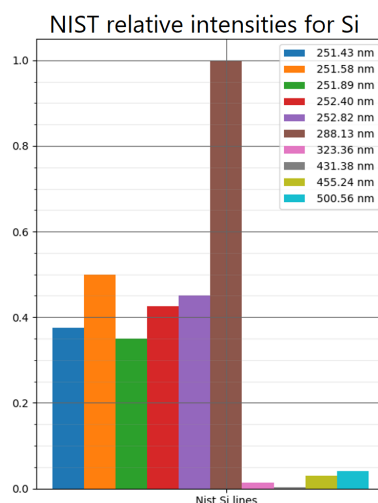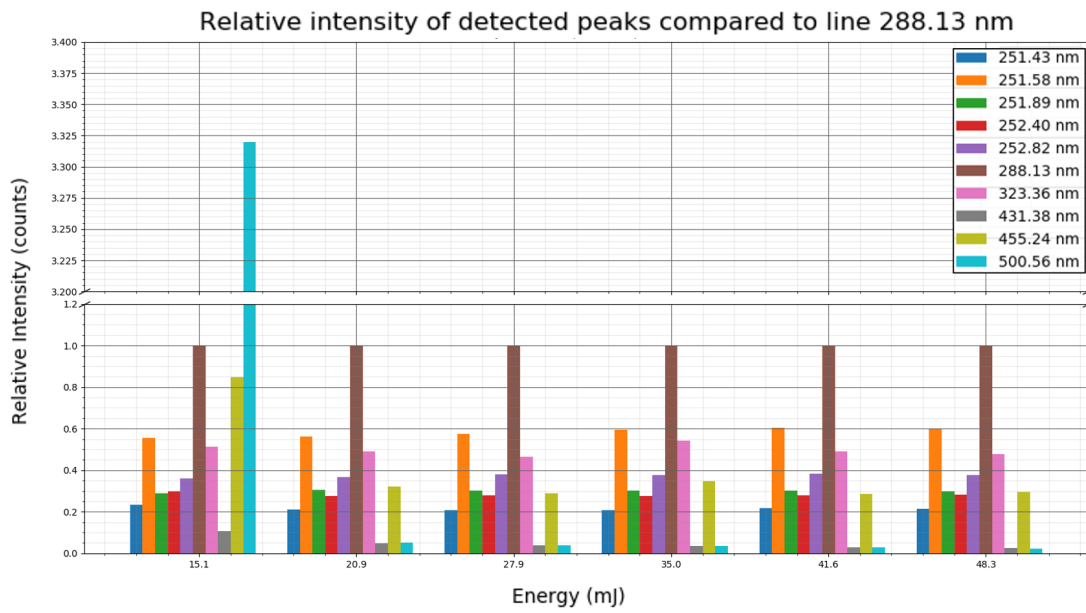
(A) Relative average intensity of Si lines detected on the first shot of 80 nodes over average intensity for line 288.13 nm. These lines were present in 80% of all spectra obtained for the first laser shot.
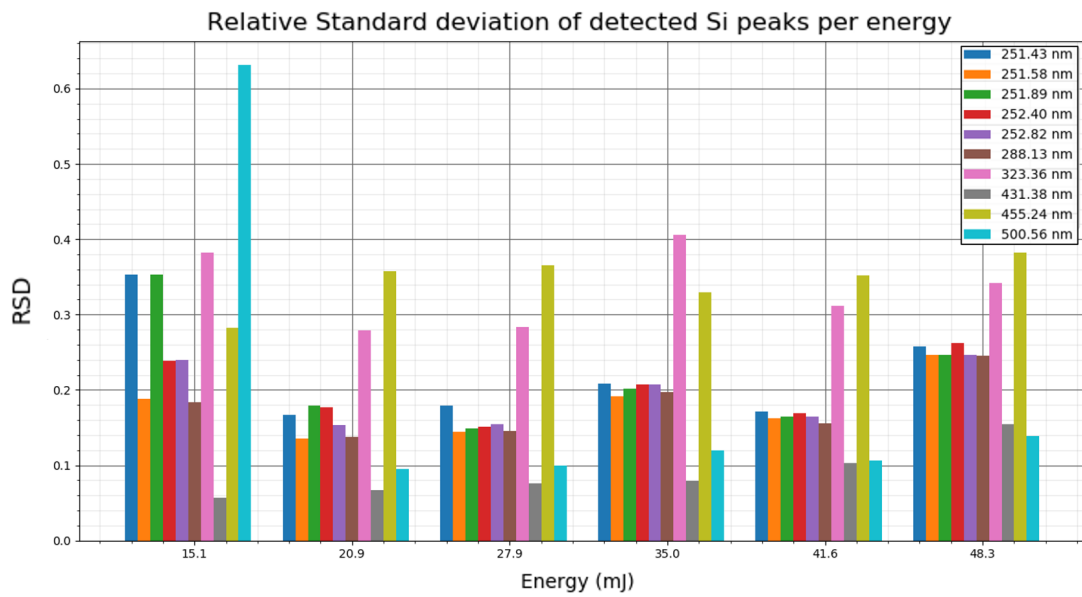
(B) Relative standatd deviation of the average signals represented in Figure A.4 as a function of pulse energy and wavelength of detected Si peaks

FIGURE 4.2: Bar representation of the relative average intensity, in counts, and the associated RSD for the detected lines of Si present in 80 % of the spectra.

those that presented less than 15% of difference between the reference and experimental intensity ratios. That leaves the wavelengths 251.58, 251.89, 252.82 and 288.13 nm as good peaks to represent Si.

From Figure 4.2 (B), it can be seen that pulse energies of 20.9 and 27.9 mJ show smaller

values of RSD in general for the chosen peaks mencioned in the previous paragraph compared to the other energy values. In addition, measurements at 15.1 mJ of energy prove not to be feasible, since the high RSD values and low signal intensity indicate that there is a high level of fluctuation for each spectrum measurement at this energy. Thus, 20.9 or 27.9 mJ of power is recommended for more accurate results due to its low RSD values, where 20.9 mJ is preferred because it has a lower standard deviation value for similar RSD value to 27.9 mJ.

The variation of the spectral intensity with the number of the laser pulse shot was also studied for each of the relevant wavelengths mentioned before. A set of measurement composed of 4 laser shots done in each of three spots per pulse energy, with same value as used in the previous measurements, was made, where Figure 4.3 shows the returned results for wavelength 288.13 nm. Figure A.9 is the result for the remaining spectral emission lines.
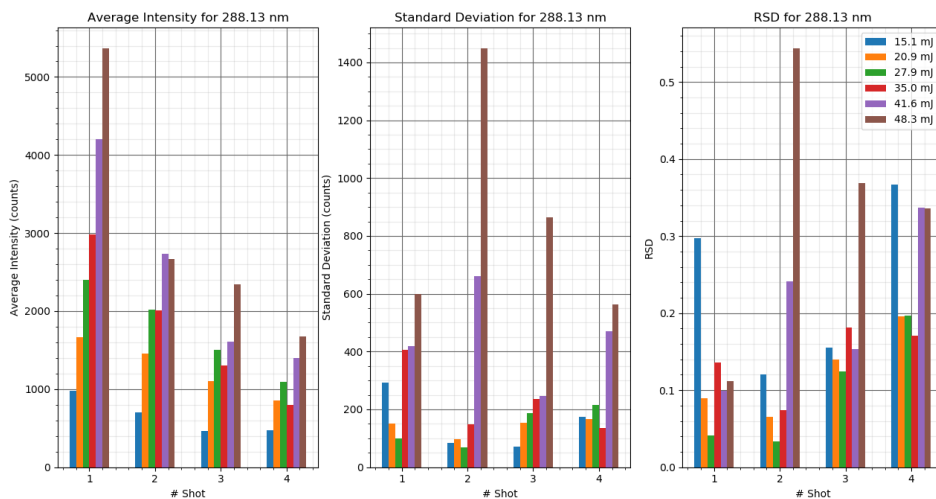
FIGURE 4.3: Average intensity, standard deviation and relative standard deviation of peak at 288.13 nm for the 4 shots made in each of the 3 nodes for each energy.

It is possible to observe that the first two laser pulse shots have a more precise result for all evaluated wavelengths, since the spectral signal is higher and the RSD value, in general, is lower compared to the other shots. This would be expected since the first and second shot remove a significant amount of material, causing loss of chemical information of the sample. Other possible influence is the fact that the incidence of the pulse in the sample happens further away with each shot made, so there is a greater loss of information when the radiation is captured.
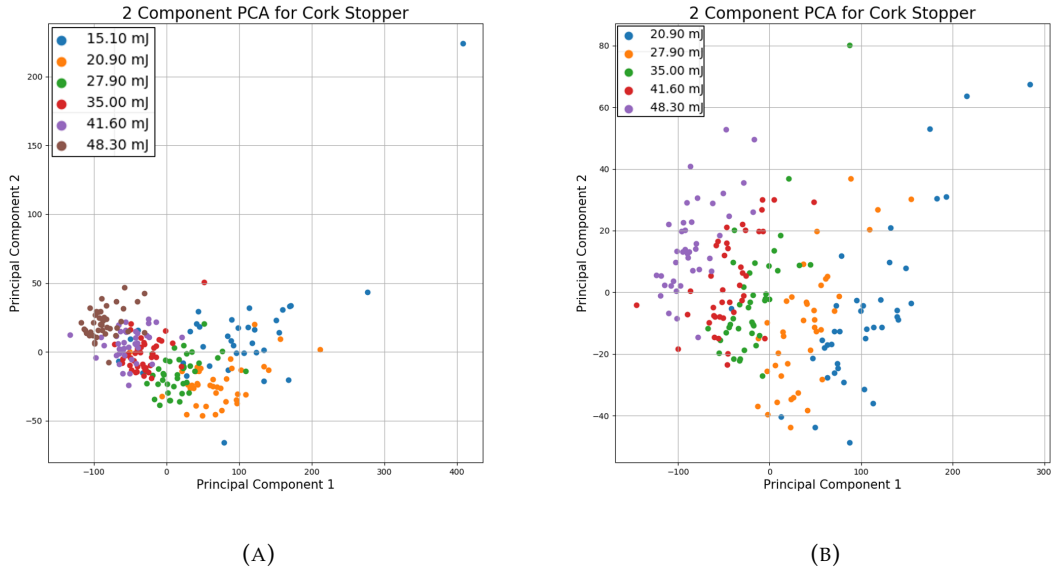
FIGURE 4.4: PCA plots using the first shot of all 40 spots made for each pulse energy values of 15.1, 20.9, 27.9, 35.0, 41.6 and 48.3 mJ. (A) is the PCA plot using all the mentioned energy values,while (B) discards the values at 15.1 mJ.

Not considering the energy of 15.9 mJ, lower energy pulses generate a cleaner signal for all studied wavelength and, for each laser shot made, the signal is of lower intensity and has greater relative fluctuation.

This observation enforces the use of 20.9 mJ pulse energies (380 μs of Q-switch delay) for the subsequent shots. This choice is due to the aforementioned low RSD value for the lines of interest, as well as the low but reliable value of average intensity, which translates in general, into a smaller standard deviation in relation to the results obtained with 27.9 mJ.

PCA method was used in the data obtained to determine if discrimination of collected spectrums by pulse energy is possible. If discrimination is indeed possible, spectra normalized according to its associated pulse energy could be used in future work. This means that data independent of the energy pulse value can be obtained, increasing the efficiency and commutability of the spectra analysis. For each energy value used, namely 15.1, 20.9, 27.9, 35.0, 41.6 and 48.3 mJ, three shots were made in 40 spots, where the recorded spectra went through the PCA method.

Figure 4.4 shows that discrimination of spectrum by pulse energy used is possible, since PCA values of same energy spectra are grouped together. Figure 4.4 (B) is the PCA plot using all but the 15.1 mJ spectra, since (A) shows that 15.1 mJ spectra are more spread

36

OPTIMIZATION OF LASER-INDUCED BREAKDOWN SPECTROSCOPY (LIBS) FOR
APPLICATION IN THE CORK INDUSTRY.
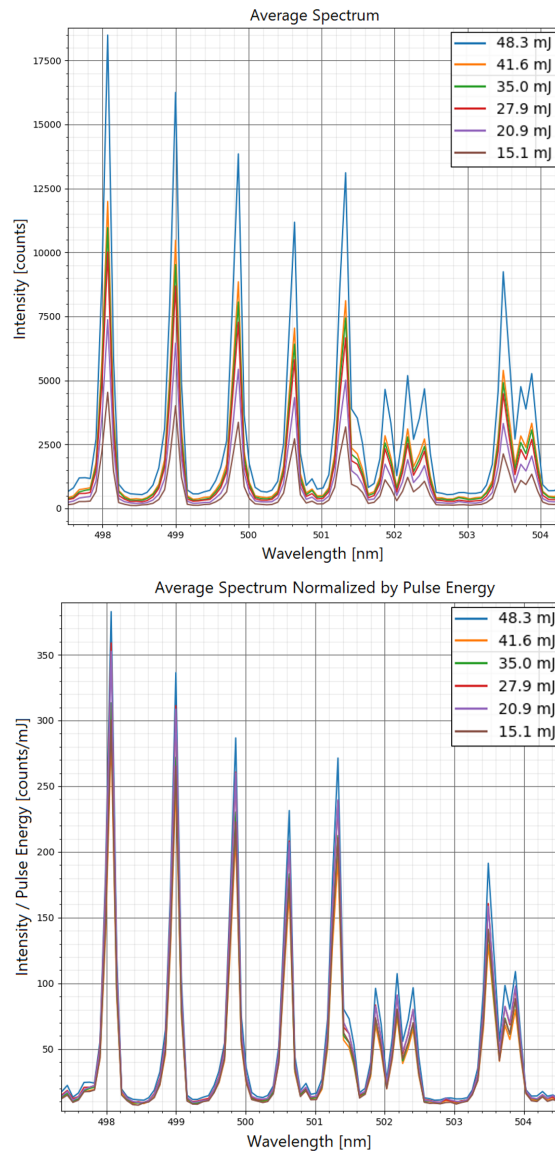
FIGURE 4.5: Comparison between average spectrum (TOP) and energy-normalized average spectrum (BOTTOM) for each pulse energy used. Normalized signal values show to be closer relative to each other in comparison to the non-normalized signals. This was visible for all wavelenght range of the spectrum.

out, meaning that their distinction from other energy values is more difficult. This is another argument for 15.0 mJ being an insufficient pulse energy for a reliable reading.

With these favorable results, comparison between the average signal intensity with and without normalization by pulse energy was made in order to observe an energy independent spectrum data. The same set of data that generated the PCA graph was used for this process. For each energy value, the average spectrum of the first shot was calculated from the forty spots in order to smooth the signal noise and remove any unwanted fluctuation. The intensity values of these average spectra were then divided by the pulse energy value

and compared with the previous values without normalization. Ideally one would expect an overlap between the peak values for the various energies.

Figure 4.5 contains the representations of a section of the non-normalized average spectrum (top) and the same section but with the average spectrum normalized by pulse energy (bottom). It can be observed that the intensity values of the different energies are closer to each other when data normalization is carried out, with almost an overlap of values. Looking at the peak at 288.13 nm wavelength in Figure 4.6, the same observation can be made, where peak values tend to approach each other when energy normalization is applied, the exception being the peak for line 288.13 nm at 48.3 mJ of pulse energy, which showed to have an abnormal behavior.
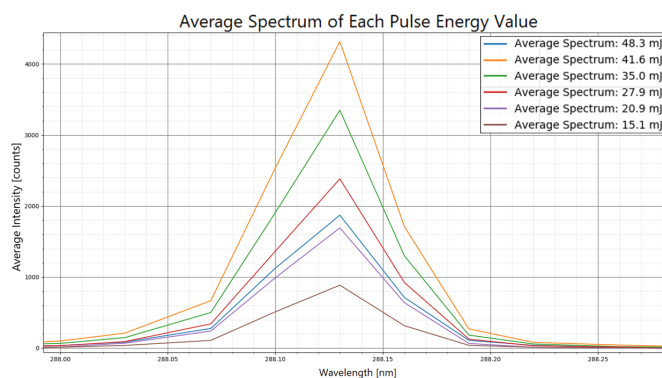
(A) Average Spectrum.
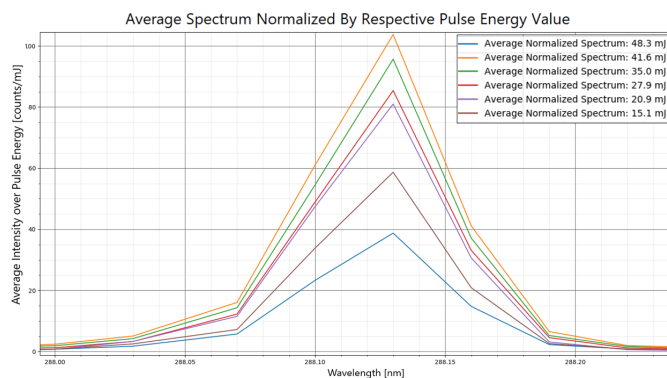
(B) Average Energy-Normalized Spectrum.

FIGURE 4.6: Comparison between disparity of average spectrum (A) and energy-normalized average spectrum (B) around 288.13 nm for each pulse energy used. It can be seen that normalized signal values of the peak at 288.13 nm are closer relativet to each other in comparison to the non-normalized signals. This was visible for all wavelenght range of the spectrum.

For a better analysis of the signal improvement using normalization, the RSD was determined for the normalized and non-normalized data using the peaks of Si at 251.58, 251.89, 252.82 and 288.13 nm of wavelength. It was expected a lower RSD value for the

normalized data, since ,ideally, the normalization would lead to the resulting signal becoming independent from the pulse energy used.
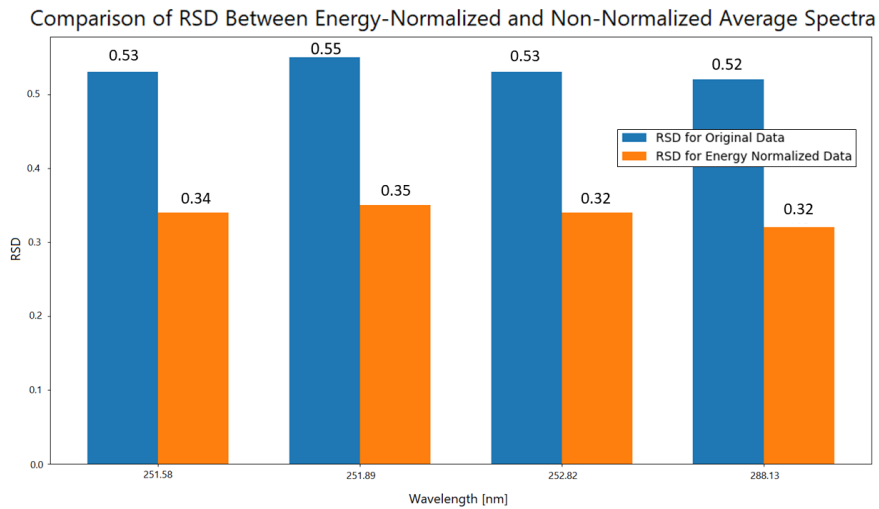

FIGURE 4.7: Comparison between RSD values using energy normalized data and nonnormalized data for wavelengths 251.58, 251.89, 252.82,288.13

As expected, the RSD value decreased when energy normalization is applied, with a drop of 38 % of the average RSD value, from around 0.53 to 0.33 (Figure 4.7). Considering that the data obtained at 48.3 mJ are outliers due to their abnormal behavior, RSD values were recalculated using only the remaining energies. In this result the RSD values between normalized and non-normalized data showed a higher difference than the one seen in the previous calculation, where the average RSD value went from around 0.54 to 0.21, as seen in Figure 4.8. This corresponds to a drop of 61%.
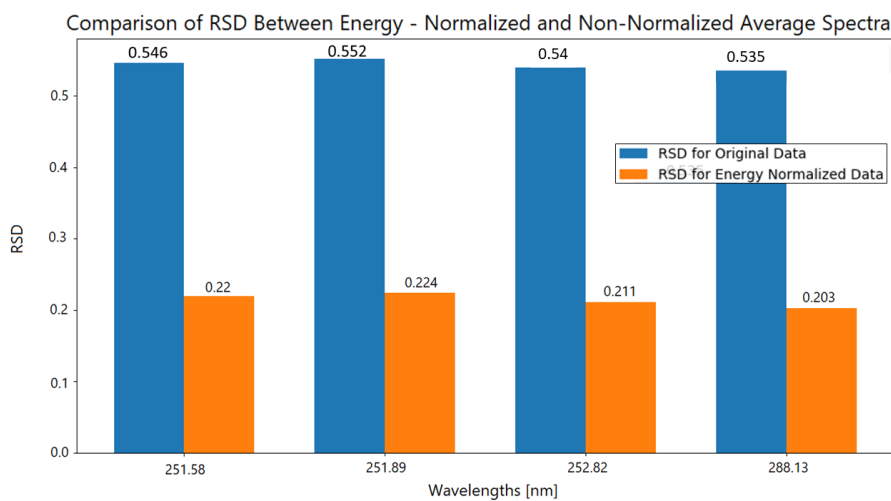
FIGURE 4.8: Comparison between RSD values using energy normalized data and nonnormalized data for wavelengths 251.58, 251.89, 252.82 and 288.13 nm, not considering the data at 48.3 mJ due to its abnormal behavior.

This increase in data accuracy is due to the peaks tending to overlap with energy normalization, as can be seen in Figures 4.9 and 4.9. Discarding pulse energy of 48.3 mJ, ratio of peak value compared to line at 41.6 mJ increases when using energy normalization, resulting in the observed decrease of RSD.
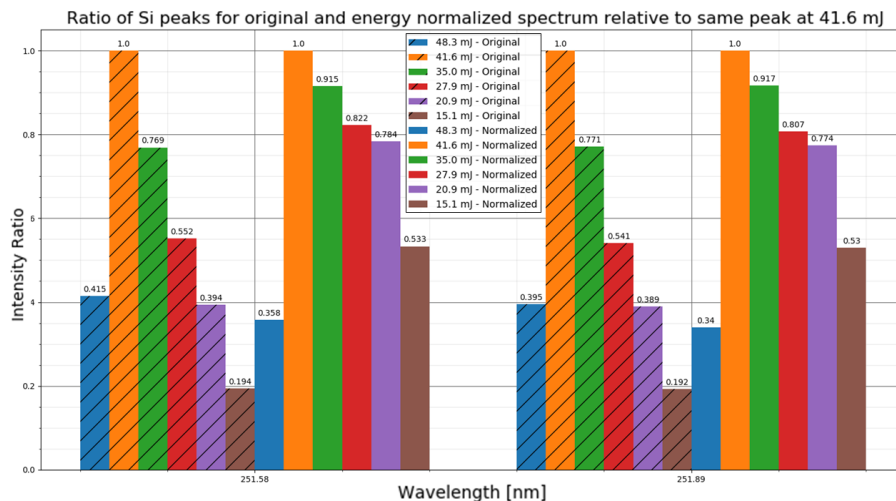
FIGURE 4.9: Spectral ratio evolution for peaks at 281.58 and 281.89 nm of wavelength when applying data normalization by pulse energy.
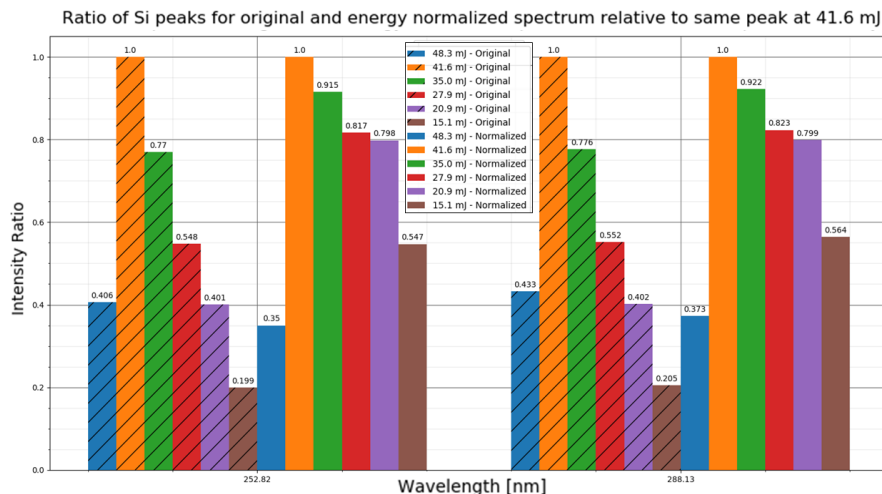
FIGURE 4.10: Spectral ratio evolution for peaks at 252.82 and 288.13 nm of wavelength when applying data normalization by pulse energy.

With this it can be concluded that the normalization of the data with pulse energy used allows for a more effective analysis of the obtained spectra, making it possible to obtain results independent from energy. Unfortunately this process has not removed entirely the energy dependency of the data. The reason for this can be attributed to the degradation of the laser source over time, the irregular profile of the laser pulse, with quality score M^2

of 5.5, and the complex nature of cork. Even so the energetic normalization of the data is advised to improve result.

4.2   Damage and Depth Study

4.2.1   Damage

In order to study the amount of damage to the stopper caused by the laser pulses, laser shots were made varying the number of shots per point and the energy of those laser pulses. Using a measurement software (IC Measure), an estimation of the damaged area caused by this combination (# *of shots* × *energy of pulse*) was measured. The parameters of # *of shots* and *pulse energy* used are in between 1 and 10 for # *of shots* and from 390 to 320 *μm* of Q-switch delay, which translates into a range of pulse energies between 15.1 and 63.0 mJ, respectively. Lower Q-switch delays from 320 *μm*, i.e. higher pulse energy values above 63.0 mJ, were not used since saturation of spectral lines was observed with these parameter values.

Estimation of the damaged area was done as follows: The smallest diameter of a circular area that contained all the damage observed at the spot was recorded (outer diameter). A diameter of the circular area where the most intense damage was done (inner diameter) was also recorded. The final value considered was the average between the two diameter values. This calculation process was carried out with the consideration that the area that appeared to be the most external of damage may be a pre-existing damage to the stopper prior to the laser firing. In this way, the average between the two diameters would return a more accurate and uniform value in contrast to the measurement using only one of the mentioned values. Figure 4.11 shows an example of the diameters measured.

The measuremets made for this study are shown in Table A.1, and graphical plots relating energy pulse and number of shots to the estimated diameter of damaged area can be seen in Figure A.2 in Appendix A. From the values of diameter obtained, Figure A.3 was also created where the area of damage is plotted against number of laser shots and pulse energy.

From the results obtained, it is possible to observe a linear relationship between the estimated diameter, and consequently the calculated area, and the energy attributed to the laser pulse ((A) of Figures A.2 and A.3). This would be expected since the size of the

(A) External diameter measured.

(B) Internal diamete measured.
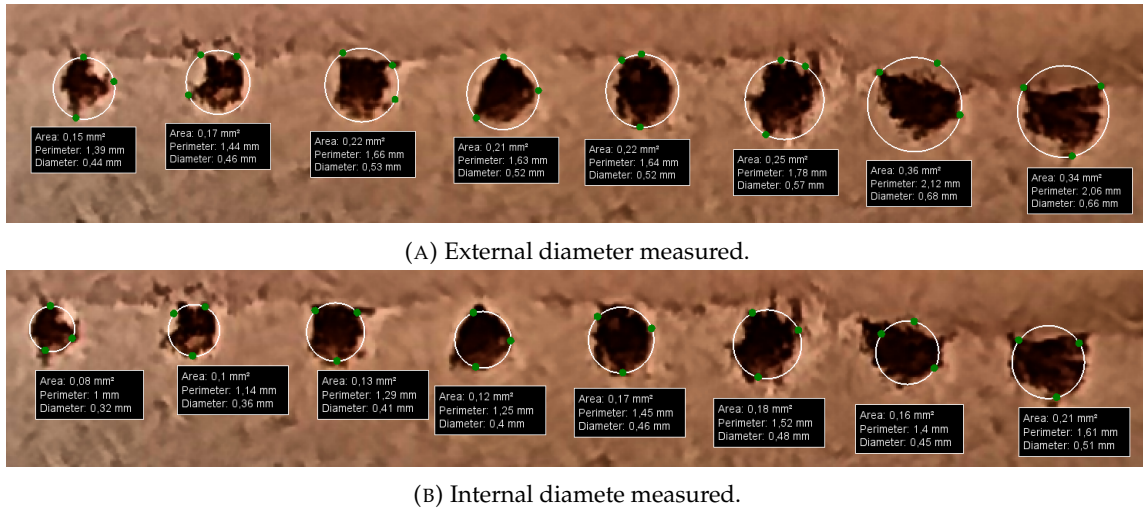
FIGURE 4.11: Example of inner and outer diameter measurements. In this case, eight laser shots were made for each spot, where the left most spot was with pulse energy of 15.1 mJ (390 μs of Q-switch delay) and the right most spot was with 63.0 mJ (or 320 μs of Q-switch delay).

plasma generated, which ablates part of the sample, increases with the increase in pulse energy.

In the case of the relationship between the damage generated and the number of shots fired ((B) of Figures A.2 and A.3), it appears to have an exponential relationship that converges to a limit value. This was also the expected result, since these measurements were made on the surface of the cork and the shots contribute less and less to this type of damage as the sample is ablated in depth. This lateral damage is due to the fact that the pulse is wide on the nanosecond scale, which leads to some lateral ablation due to the wings present in the pulse profile. In the case of a femtosecond pulse, this lateral ablation would be practically imperceptible due to its narrower profile width.

This study is also useful for choosing step value between spots so that the adjacent spot is not located in an area already damaged or with material deposited from the previous shots. The areas obtained were compared with a square area defined by steps of 0.5 mm and 1 mm, for comparison with the area the laser pulse has avaliable before damaging (Table 4.1). It was decided that the best step is 1 mm, so that there is a good margin of maneuver for possible deviations from the motorized stage, laser or the presence of damage and deposited material. Plus working with round numbers is more pleasing. In the section related to mapping, we will talk more about the step and their influence on the obtained maps.

42

OPTIMIZATION OF LASER-INDUCED BREAKDOWN SPECTROSCOPY (LIBS) FOR APPLICATION IN THE CORK INDUSTRY.

	Energy (mJ)	15.1	20.9	27.9	35.0	41.6	48.3	56.0	63.0
Step (mm)	0.5 Min %	3	4	2	6	10	10	13	16
	0.5 Max %	48	54	70	80	87	95	100	108
	1.0 Min %	0.9	1	0.6	1	2	3	3	4
	1.0 Max %	12	14	17	20	22	24	25	27

TABLE 4.1: Minimum and maximum values of damaged area ratio compared to an area with step 0.5 mm and an area with step 1.0 mm. Minimum values are associated with first shots, while maximum are for the latter shots. It can be seen that, for step of 0.5 mm, area available may not be enough so as to not hit a damage or deposited area in the next spot.

4.2.2 Depth

The vertical damage caused by laser pulses was also observed in order to calculate an estimation of the ablation performed by each energy shot. Since the ablation performed by one shot is too small to study individually, twenty laser pulses were performed per spot, at 3 different spots, for the same pulse energy, for energy values of 20.9, 27.9, 35.0, 41.6 and 48.3 mJ. The cork stopper used contained a Si coating. Damage done by 15.1 mJ laser pulses were not possible to measure due to the difficulty in discriminating the cavity from the surrounding material. Figure 4.12 shows an example of an image of the cavity used to measure its depth.
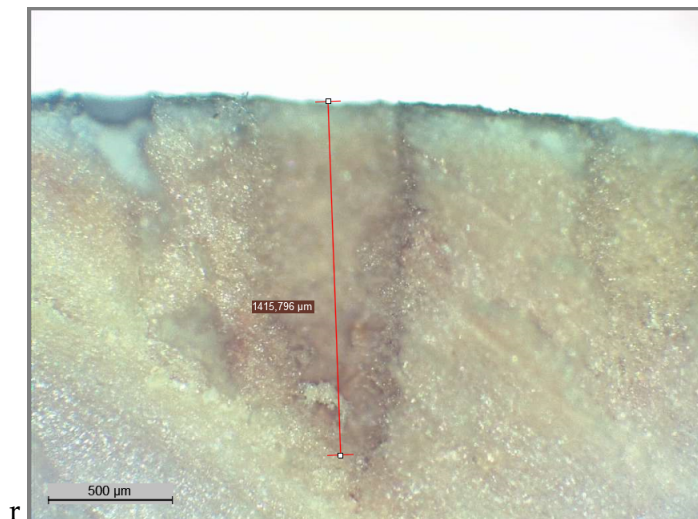
FIGURE 4.12: Example of a measurement made to determine depth of cavity using a laser pulse of energy 48.3 mJ.

Due to the non-availability of adequate equipment and the time and displacement restrictions, the measurement of vertical damage was done using a model microscope equipped with a camera recorder and with the help of a measuring software program.

To observe the ablation under the microscope, a careful cut was made in order to split the ablated zones into two equal parts, so that two depth measurements can be made for the same cavity. Using the measurements that obatined, the average of the ablation made by the twenty shots for each energy value was calculated. The single shot ablation was estimated by dividing the total average depth by the total number of shots, in this case it was twenty shots. Table 4.2 shows the average of the measurements made in each pulse energy for the twenty shots, the RSD value of those measurements and an estimation of the average ablation done by one shot with the certain pulse energy. The measurements made are in Table A.4 of Annex.

Energy [mJ]	Average Depth [μm] (20 Pulses)	RSD (%)	Average Ablation per Pulse [μm]
20.9	712	8	36
27.9	993	4	50
35.0	860	10	43
41.6	1114	4	56
48.3	1341	6	67

TABLE 4.2: Average values of the ablation done by twenty laser pulses in each point, and average ablation per pulse. This average was made using 3 points for each value of energy, were each point could give two measurements since it was made in both sides of the cut over the cavity.

With this simple method it was possible to have an estimation of the order of magnitude caused by a single shot. In the future depth measurement could be made using a more efficient method and measuring system, such as Atomic Force Microscopy. With a good estimation of the vertical ablation done by one laser pulse, coating thickness measurements could be made by searching in which consecutive pulse the Si spectral lines are negligible, thus being able to estimate the coating thickness.

OPTIMIZATION OF LASER-INDUCED BREAKDOWN SPECTROSCOPY (LIBS) FOR
APPLICATION IN THE CORK INDUSTRY.

44

4.3 Influence of Clean Shot

Another pertinent question that came up when determining methods to improve spectral data was whether a low energy shot, i.e. a clean shot, prior to the main shot would be useful to decrease data fluctuations. For this purpose, spectra colected using clean shots prior to the main laser pulse were compared to spectra from measurements made without clea shot.

A set of measurements made in 20 points of a Si-coated stopper were made using two consecutive laser pulse shots, each preceded by a clean shot with pulse energy equal to 3.7 mJ (or 410 s of Q-switch delay), resulting in a total of four shots per spot. Using the data recovered here and the data from the previously used 80 points measurements made for the energy study, the average value and standard deviation of both sets were compared, where the data from the 80 points were unfolded into 4 groups of 20 nodes in order to make a fair comparison.

Figure A.10 in Annex shows the results of the average intensity, standard deviation and relative standard deviation obtained from spectral peaks of Si at 251.58, 251.89, 252.82 and 288.13 nm for the four groups of measurements made without clean shot and the group made with clean shot of 3.7 mJ of pulse energy before every main shot. Contrary to what was expected, the precision of the data is significantly higher for measurements made without the use of a clean shot,where the RSD values for the first shot were between 0.1 and 0.2, and these rose to a range between 0.2 and 0.25 when the clean shot was used. For the second main shot the accuracy decreased as expected, with a loss of accuracy of about 10 % in both cases, keeping the data without using clean shot as the most accurate between the two sets. This can be attributed to the fact that the clean shot, although of low energy, destroys part of the sample in that point, which will influence the spectrum recorded by the next main shot. However, a clean shot may be beneficial in the scenario where the sample to be analysed contains impurities in order to remove them at that point for a good record of the spectrum at the next shot

4.4 Mapping Cork Stoppers

To determine the quality of distribution of coating over the stopper, LIBS measurements can be made so as to obtain spectra from a desired area of the sample and elaborate an uniformity map from the data acquired. For coatings with distinct chemical elements from

the stopper material, this can be done by looking at the signal intensity of spectral lines unique to the coating. In the cases where there isn't a characteristic line that discriminates stopper and coating, PCA was considered in making uniformity maps of the coating of the stoppers. In order to determine if PCA can be used for this purpose, uniformity maps using both methods in a Si-coated natural cork stopper were made and compared to each other.

4.4.1   Cork Mapping by Spectral Peak Intensity

Measurements were made on a new Si-coated cork stopper, named B1, where a tape was placed prior to its treatment, thus creating an uncoated band when the tape is removed. Six shots were performed with pulse energy of 20.9 mJ over 200 spots with step of 2 mm in a 20×10 configuration.

Figure 4.13 shows the expected coating distribution (A) and the uniformity map obtained from the B1 stopper for peak at 288.13 nm wavelength at the first (B), third (C) and sixth (D) laser pulse shot. The maps obtained using the wavelengths 251.58, 251.89 and 252.82 nm are represented in Figures A.12, A.13 and A.14, respectively, placed in Annex.

In them a strip of very low signal intensity is observed compared to the rest of the map, corresponding to the area of the stoppernot covered by Si coating. It can also be seen that, although signal intensity of Si-covered areas decrease over multiple shots, it's still possible to discriminate the area not covered by Si coating in subsequent shots until enough coating is removed and laser pulse reaches the cork stopper.

4.4.2   Cork Mapping using PCA method

For more complex coatings, where there is no spectral line uniquely characteristic the coating or the cork stopper, the maping by intensity line is not suitable. This is the case for natural cork stoppers treated with a paraffin coating. In this scenario, cork and paraffin have elements in common between the two, since cork is a biological product consisting mainly of carbon, oxygen and hydrogen, while paraffin has a chemical composition equal to $C_nH_{2n+2}(n > 20)$. Oxygen is unreliable since LIBS plasma could ionize the surrounding air, emitting oxygen spectral lines not associated to the cork stopper.

The solution considered was the implementation of the PCA method to the spectra obtained and to elaborate uniformity maps from the values of the principal components (PC1, PC2, ...) returned by the method. Initially this process was carried out in Si-coated

(A) Expected uniformity map. Blue represents the area without silicon coating.

(B) Laser pulse shot number 1.

(C) Laser pulse shot number 3.
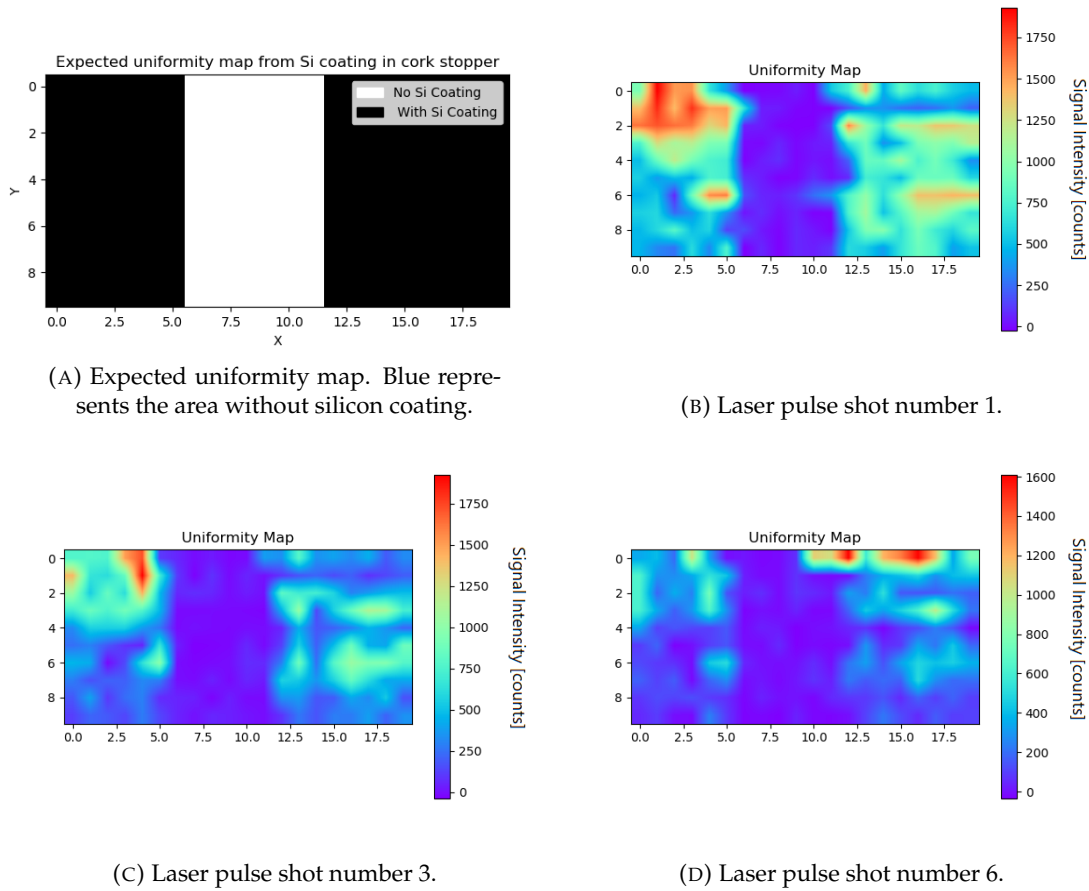
(D) Laser pulse shot number 6.

FIGURE 4.13: Uniformity map expected (A) and obtained by looking at the 288.13 nm peak of the spectrum for a cork stopper with Si coating for shot 1 (B), 3 (C) and 6 (D). A slight absence of signal can be seen in the center part of the plot, representing the area with absence of Si coating.

natural cork stopper. Using the same spectral data used in Figure 4.13, the maps obtained by PCA were compared to the reference maps obtained with the signal intensity of Si lines. Obtaining a map of uniformity similar to the reference map was the desired outcome and a good start to implement this process in the paraffin-coated stopper.

The process to obtain the map using the PCA method was the following: the intensities of the entire wavelength range of the spectrum, for shots of same number, were grouped and PCA method was performed on them. With the respective principal component value associated to each laser pulse shot, 2D plots were generated using PC1 and PC2 values, where each coordinate (x,y) of the plot contained the PC value of the associated spot. Figure 4.14 shows the result obtained with this process applied to the first shot of all spots of the B1 stopper.

The resulting plot obtained from PC2 values suggests the existence of a central zone
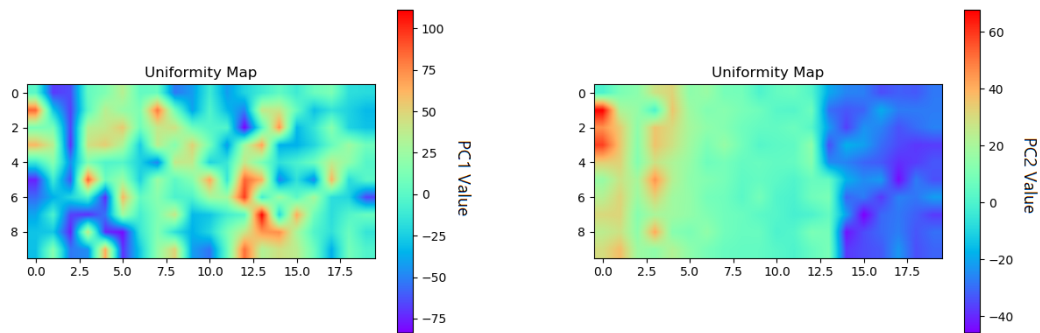
(A) Uniformity map using PC1 values obtained for Si-coated stopper spectrum data.

(B) Uniformity map using PC2 values obtained for Si-coated stopper spectrum data.

FIGURE 4.14: Uniformity map obtained using PCA method using PC1 and PC2 for all wavelength range of the data.

between two areas of opposite value of PC2. Looking at the absolute value of PC2 values (Figure 4.15), a central zone similar to the one seen in Figure 4.13 and situated approximately in the same coordinate range is observed. The same area is detected in subsequent laser shot number up until shot number five, due to the ablation already suffered up to that point (Figures A.15a through A.15e in Annex).
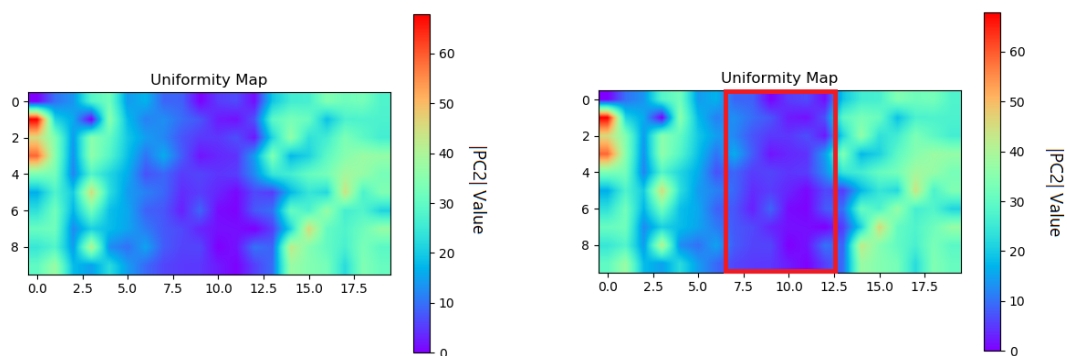
FIGURE 4.15: Uniformity map obtained using using norm values of PC2 for all wavelength range of the data (Left). An area of lower PC2 norm value is visible (Right), located approximately in the same area as the one detected in Figure A.14a.

The maps obtained are within what would be expect when using this method. The reason for its greater imprecision to discriminate the boundaries of the uncoated silicon area can be attributed to the fact that the PCA method considers all 16384 recorded wavelengths for the same number of shots and reduces the data dimension to the two with higher variance, while specral peak mapping, that returned Figure 4.13b and Figures A.12
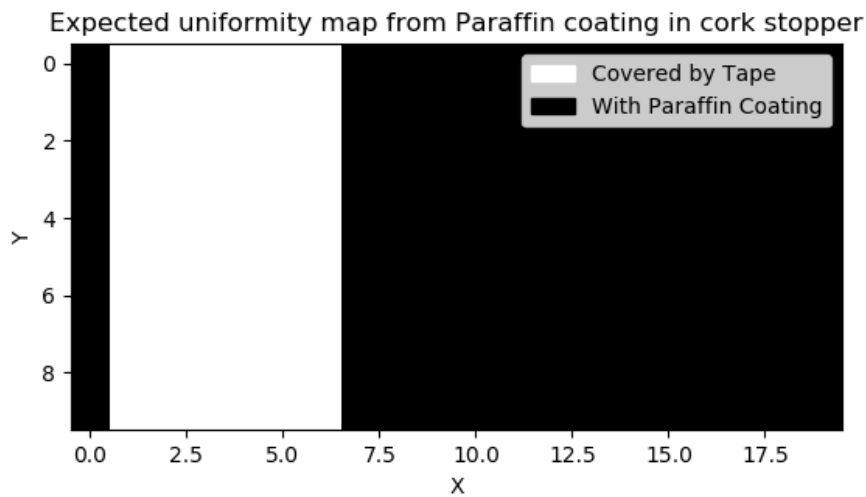
FIGURE 4.16: Paraffin coating distribution of a cork stopper with area covered with tape.

throught A.14 in Annex, only uses the intensity of a single spectral line. Even so, mapping using PCA showed to be possible.

With these favorable results, the next step is to obtain the uniformity map of a cork stopper with paraffin coating, to verify indeed the viability of this process. An adhesive tape was placed along the stopper, in order to replicate an area without paraffin coating. For this analysis, six consecutive shots were made in the same spot along 150 points in a 15×10 configuration with 2 mm of step. The energy of the laser pulses was again adjusted to 20.9 mJ of energy.
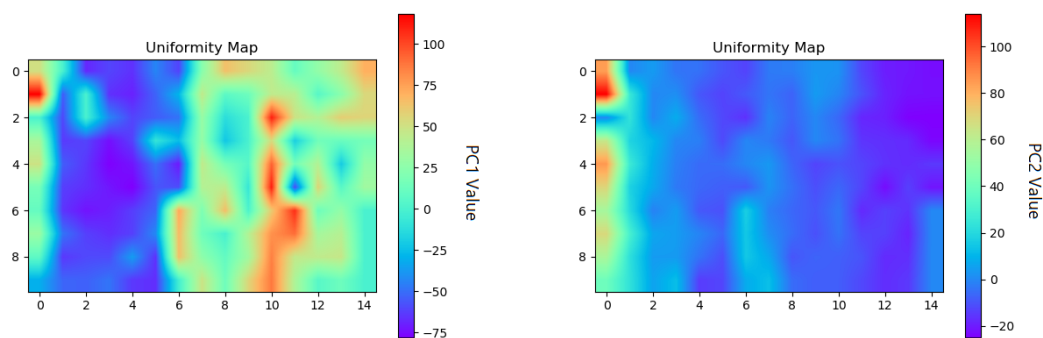
(A) Uniformity map using PC1 values.

(B) Uniformity map using PC2 values.

FIGURE 4.17: Uniformity map of shot number 2 obtained using PCA method on the data from a Paraffin-coated stopper.

Figure 4.16 represents the distribution of Paraffin coating, while Figure 4.17 and Figures A.16a throught A.16e of Annex contain the uniformity maps obtained using PC1 and PC2 for the paraffin-coated stopper. Contrary to what occurred in the PCA mapping of the stopper with silicon coating, the adhesive tape placed on the paraffin-coated stopper was identified in the PC1 mapping in all the shots made. Although this map discriminates paraffin-coated areas from the tape-covered area, PCA shows once again its surface mapping capabilities.

To better observe the difference between paraffin-coated and paraffin-free areas, a stopper was made by joining two halves of paraffin (right side) and paraffin-free (left side) natural cork stoppers (Figure 4.18).

(A) Cork stopper used.

(B) Paraffin coating distribution of the area of cork stopper where LIBS was performed 4.18a.
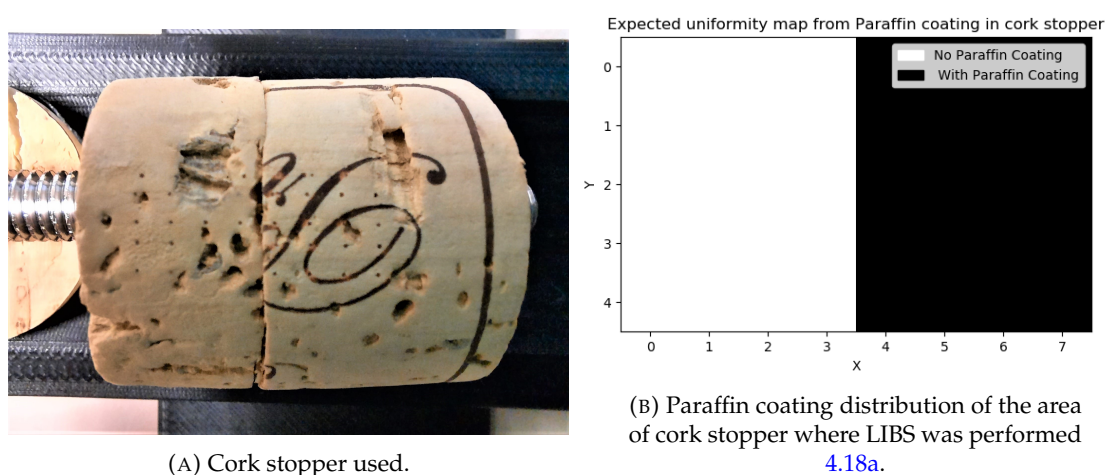
FIGURE 4.18: Stopper made from two halves of a stopper with and without paraffin coating. The shots were spaced so as to not focus on the separation between the two halves.

For the mapping of a section of the cork that encompasses both halves, a rectangular mesh of 8x5 spots was defined, where the separation is situated at half length. The separation used between spots was 2 mm, where six consecutive laser shots with a pulse energy of 20.9 mJ were performed for each spot.

A first analysis using PCA showed the existence of outliers that affect the resulting map. For a better result without significant loss of data, the spectra whose principal component value PC1 lies in the range $]-1.5\sigma; 1.5\sigma[$ were considered for the new map, where σ is the calculated standard deviation. This corresponds to a confidence interval of approximately 87 %.

The maps obtained with this method are present in Figure 4.19 and Figure A.17 in

50

OPTIMIZATION OF LASER-INDUCED BREAKDOWN SPECTROSCOPY (LIBS) FOR
APPLICATION IN THE CORK INDUSTRY.

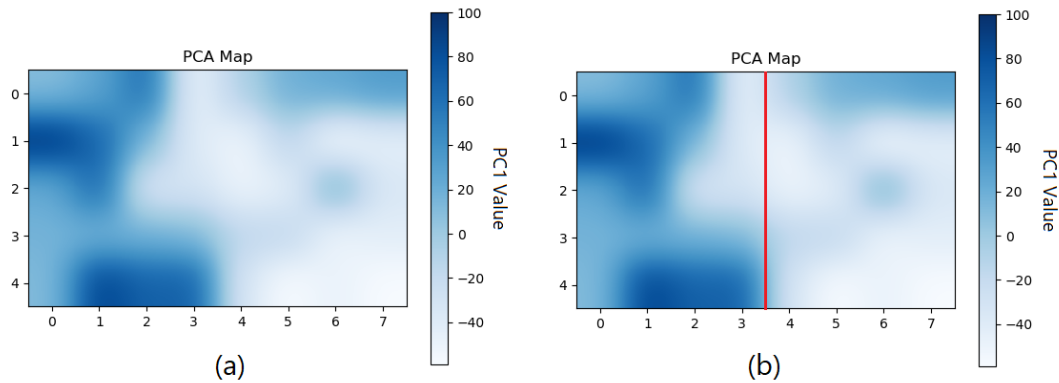FIGURE 4.19: Uniformity map obtained using the fifth shot of each node (a). Two distinct areas can be distinguished on the left and right side of the map, which goes according to the expected. The red line in (b) corresponds to the position of the interface between the two halves of the cork. This particular map came with a 80% of correspondence with the expected result.

Appendix, where two distinct areas can be observed. These areas correspond to the sections of the stopper with and without paraffin. With the results obtained, the percentage of correspondence was determined by comparing the obtained results with the expected. This calculation returned a percentage value in between 60 and 80% for the different uniformity maps , i.e. between 60 and 80% of the spots were correctly classified has having or not having paraffin coating.
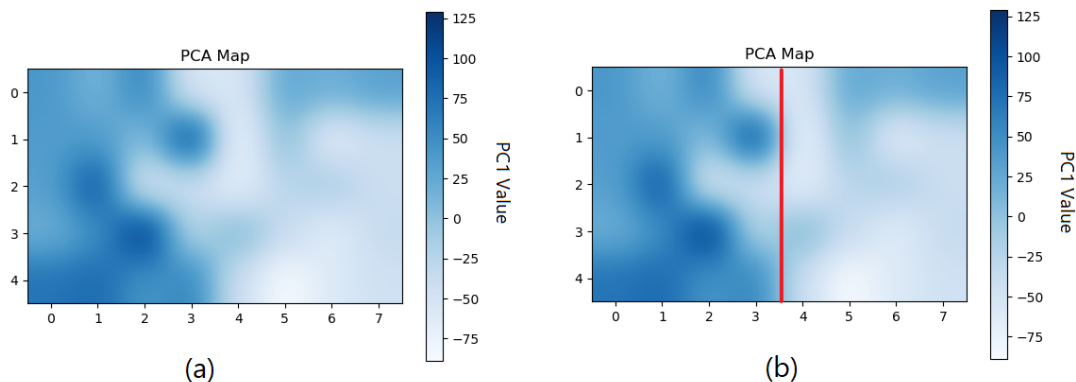
FIGURE 4.20: Uniformity map obtained using the average spectrum obtained in each spot (a). Two distinct areas can also be distinguished on the left and right side of the map. The red line in (b) corresponds to the position of the interface between the two halves of the cork. This particular map came with a 77.5% of correspondence with the expected result.

The map in Figure 4.20 was the result of using the average spectrum of all the spectra collected from the laser shots done in each spot. In this map it was possible to correctly

FIGURE 4.21: Map obtained using PC2 values from average spectrum of each spot (a). The shaded areas (delimited in (b)) correspond to the places where medium or high dimension cavities are present in the cork.

identify 80% of the paraffin zone and 75% of the paraffin-free zone, which returns an average of 77.5% of correspondence with what was expected, increasing the acuracy of the uniformity map relative to the method used in Figure 4.19.

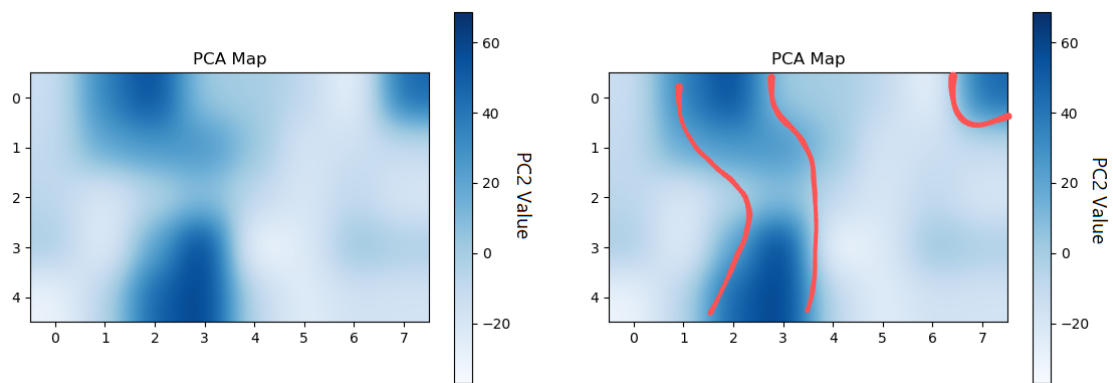In addition to detecting the presence of coating on the cork stopper, PCA mapping was also capable of detecting imperfections. Observing the map obtained with the PC2 values, shaded areas are visible in coordinates where cavities of medium to high diameter are present in the stopper, as can be seen in Figure 4.21. This observation is proven when the map obtained is superimposed onto the image of the area where the shots were made, as represented in Figure 4.22.
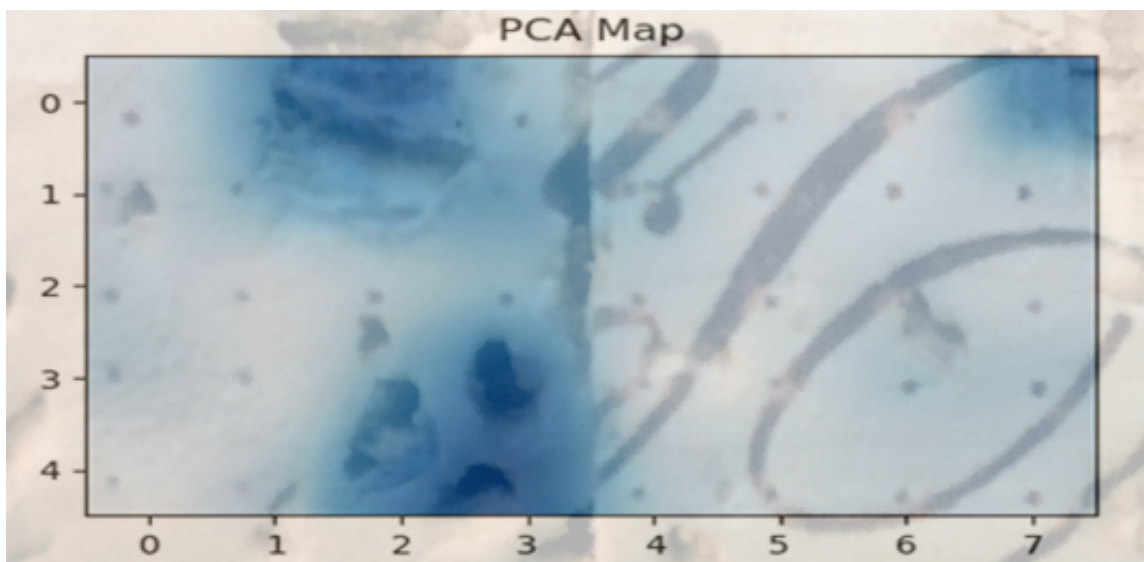

FIGURE 4.22: Overlay of the map obtained onto the image of the spots on the cork where the laser shots were made. The shaded areas coincide with the places where cavities of medium or high dimension exist, indicating that the map allows to identify imperfections on the cork surface.

All of the results obtained in the mapping procces using PCA method indicate that this method can be successfully applied in uniformity evaluation, being able to show the coating distribution as well as imperfections in the surface of the sample. Since it takes into account the whole recorded spectrum, this process shows promise in mapping more chemically complex samples where there are no unique elements in the sample or coating.

As future work, more detailed studies of PCA mapping and further data processing can be elaborated in order to improve the resulting measurements and maps of uniformity, so as to increase the accuracy of the results.

4.5   Conclusion and Future Work

The aim of this thesis was to optimize an existing system for cork analysis and to create uniformity maps, in order to study the quality of the protective coating that is placed during the production of cork stoppers. Several parameters were optimized in order to find the best parameter values that return the signals with good precision.

With this work, it was concluded that the ideal parameters to obtain results with a good degree of precision and little damage from natural coated corks for the setup used are: a minimum pulse energy of 20.9 mJ and no clean shot required. This combination of parameters has proven to be ideal for obtaining the lowest RSD value in the recorded data, translating this into good accuracy in the desired results. This energy has also proven to be the least damaging in obtaining viable data. It was also concluded that the collected spectra can be normalized by the pulse energy used, so as to eliminate, totally or partially, the energy dependence of the spectra, contributing to a greater reliability between the spectra of different pulse energies.

For the mapping of the uniformity of the coating, the PCA method proved to be viable for mapping, since the map obtained from a Si-coated cork with a band without Si returned similar results to the map obtained using the intensities of the specral lines of silicon. Applying this process to a stopper composed of one half with paraffin coating and the other half without, it was possible to identify the two zones correctly with a percentage of correspondence equal to or greater than 60%, and this value rose to 77.5% when considering the average spectrum of each spot. The imperfections present in the cork surface were also observed in maps obtained with the second main component, PC2.

Both the favorable comparison of the two methods in mapping the Si-coated cork stopper and the maps obtained from the paraffin-coated stopper show that PCA can be

used in uniformity evaluation with a good degree of accuracy, degree which can be even higher when implementing more accurate data processing tools and methods.

For future work, the aim is to optimise the processes developed in Python in order to carry out signal processing more quickly and accurately. Similarly, it is intended to optimize the mapping of the uniformity of PCA coatings and compare the results obtained and new results with other similar processes, such as Common Component Analysis (CCA), in order to obtain a greater degree of accuracy in future results, not only to better observe the distribution of coatings but also to identify inaccuracies in the samples. Depth profile studies will also be carried out to a greater extent in order to incorporate the evaluation of the coating thickness.

This future work could culminate in the development of a specialised LIBS prototype system to be used in the evaluation and analysis of various cork stoppers and its coatings in the cork industry, where the ideal parameters of each sample would be used to obtain highly accurate results. This prototype would be developed with attention to the minimum energy density required, the adequate spectrometer resolution, the the dimensions of the system and other relevant features in order to obtain a good cost-effective system for detailed analysis in cork stoppers.

Appendix A

Complementary Information

Q-switch delay (μs)	410	400	390	380	370	360	350	340	330	320	310
Energy (mJ)	3,7	6,9	15,1	20,9	27,9	35	41,6	48,3	56	63	72,1

FIGURE A.1: Energy associated with the variable Q-switch delay selected manually or through the developed scripts.

A.0.1 Damage Study

| Energy (mJ) #Shots	15.1	20.9	27.9	35.0	41.6	48.3	56.0	63.0
2	0.105	0.11	0.085	0.135	0.175	0.18	0.205	0.225
3	0.215	0.195	0.225	0.265	0.325	0.33	0.315	0.35
4	0.215	0.305	0.295	0.3	0.365	0.42	0.385	0.455
5	0.255	0.275	0.315	0.355	0.405	0.395	0.425	0.445
6	0.3	0.345	0.365	0.395	0.43	0.43	0.435	0.52
7	0.315	0.315	0.35	0.375	0.41	0.44	0.415	0.46
8	0.38	0.41	0.47	0.46	0.49	0.525	0.565	0.585
9	0.36	0.4	0.415	0.505	0.525	0.55	0.56	0.56
10	0.39	0.415	0.37	0.455	0.5	0.505	0.555	0.55

TABLE A.1: Average diameter obtained, in mm, of the area containing the damage, with error of ∓ 0.001 mm Shots #1 were not measured due to the difficulty in observing the damaged area.

Energy (mJ) # Shots	15.1	20.9	27.9	35.0	41.6	48.3	56.0	63.0
2	0.009	0.010	0.006	0.014	0.024	0.025	0.0333	0.040
3	0.036	0.030	0.040	0.055	0.083	0.086	0.078	0.096
4	0.036	0.073	0.068	0.071	0.105	0.139	0.116	0.163
5	0.51	0.59	0.78	0.099	0.129	0.123	0.142	0.156
6	0.071	0.093	0.105	0.123	0.145	0.145	0.149	0.212
7	0.078	0.078	0.096	0.110	0.132	0.152	0.135	0.166
8	0.113	0.132	0.173	0.166	0.189	0.216	0.251	0.269
9	0.102	0.126	0.135	0.200	0.216	0.238	0.246	0.246
10	0.119	0.135	0.108	0.163	0.196	0.200	0.242	0.238

TABLE A.2: Areas, in mm^2 associated with values of Table A.1

Energy (mJ) # Shots	15.1	20.9	27.9	35.0	41.6	48.3	56.0	63.0
2	1.65E-04	1.73E-04	1.34E-04	2.12E-04	2.75E-04	2.83E-04	3.22E-04	3.53E-04
3	3.38E-04	3.06E-04	3.53E-04	4.16E-04	5.11E-04	5.18E-04	4.95E-04	5.50E-04
4	3.38E-04	4.79E-04	4.63E-04	4.71E-04	5.73E-04	6.60E-04	6.05E-04	7.15E-04
5	4.01E-04	4.32E-04	4.95E-04	5.58E-04	6.36E-04	6.20E-04	6.68E-04	6.99E-04
6	4.71E-04	5.42E-04	5.73E-04	6.20E-04	6.75E-04	6.75E-04	6.83E-04	8.17E-04
7	4.95E-04	4.95E-04	5.50E-04	5.89E-04	6.44E-04	6.91E-04	6.52E-04	7.23E-04
8	5.97E-04	6.44E-04	7.38E-04	7.23E-04	7.70E-04	8.25E-04	8.87E-04	9.19E-04
9	5.65E-04	6.28E-04	6.52E-04	7.93E-04	8.25E-04	8.64E-04	8.80E-04	8.80E-04
1	6.13E-04	6.52E-04	5.81E-04	7.15E-04	7.85E-04	7.93E-04	8.72E-04	8.64E-04

TABLE A.3: Uncertainties associated with the calculation of damaged area, in mm^2 for values of area in Table A.3.
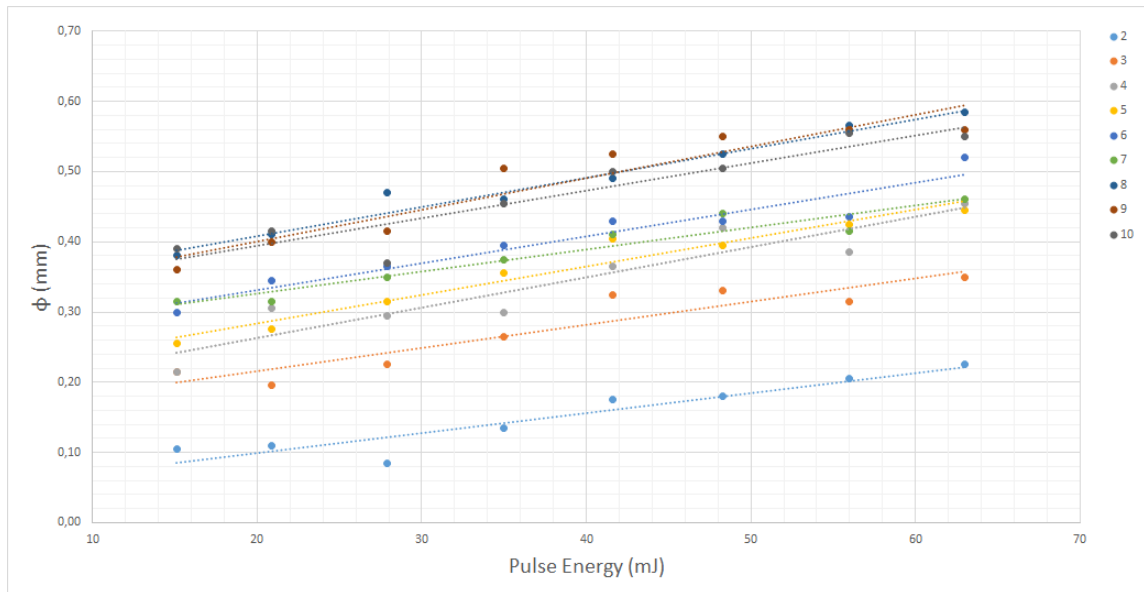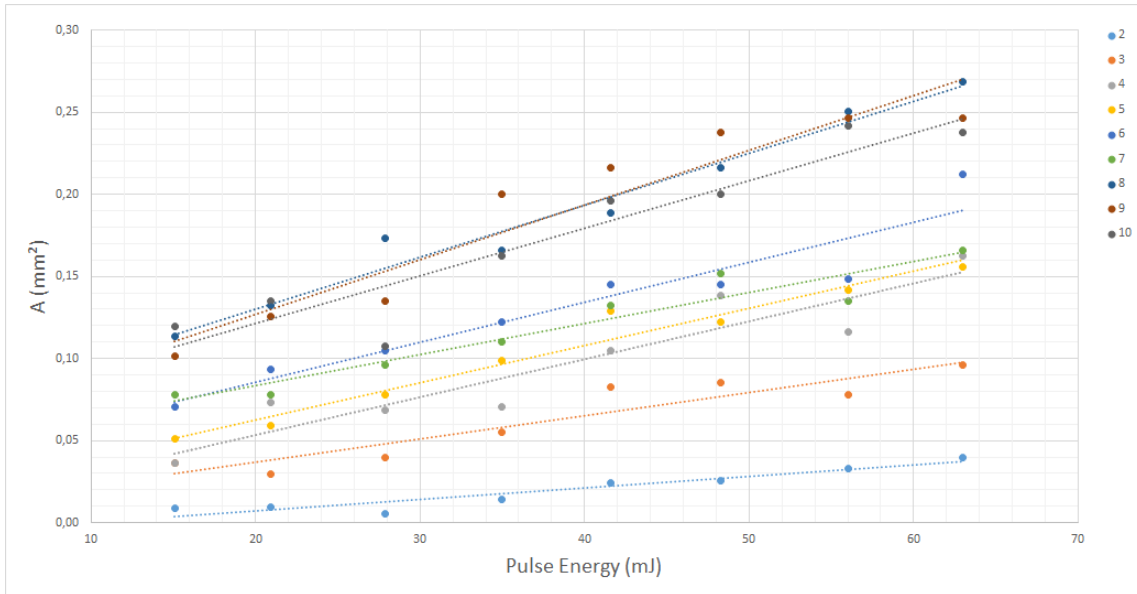
(A) Diameter of the damage area relative to the energy of the shots for each shot number (legend).
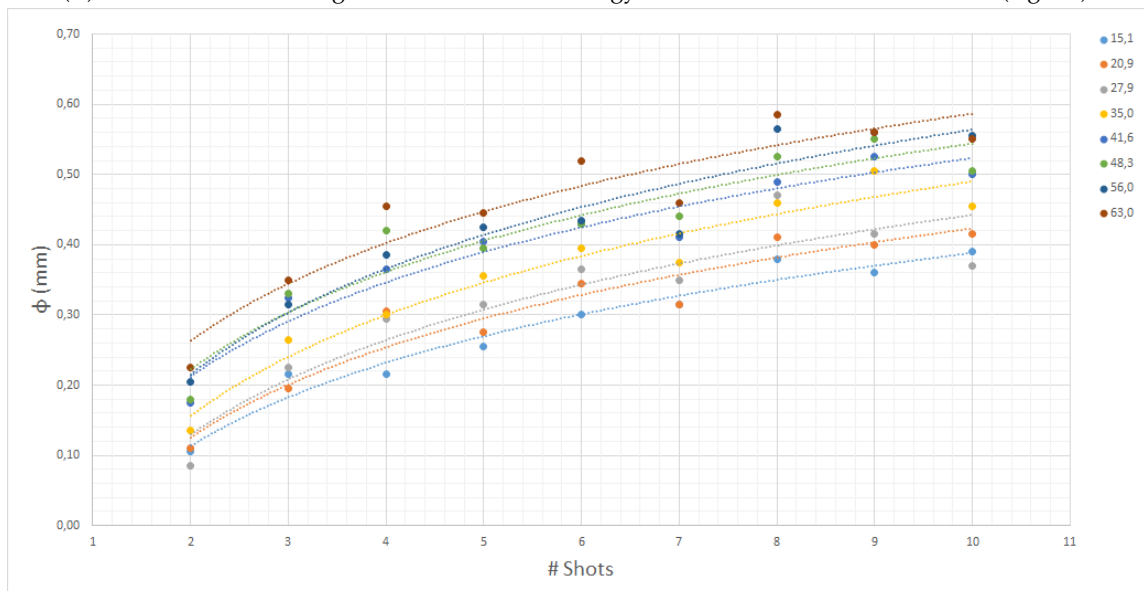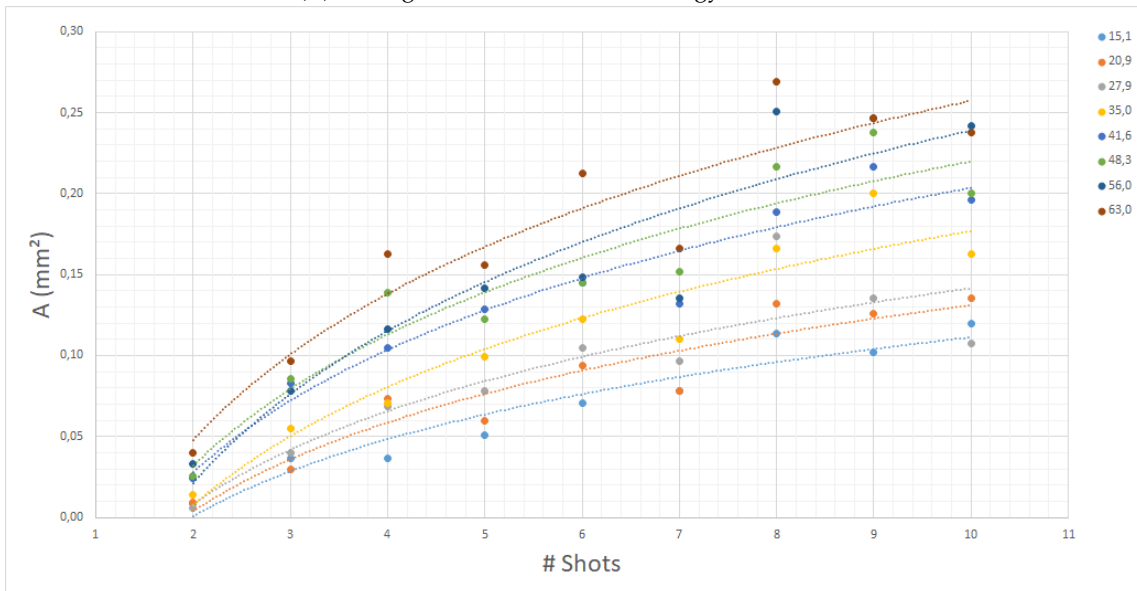

(B) Diameter of the damage area relative to the number of shots done in a spot for each pulse energy (legend) in mJ .

FIGURE A.2: Plots for the average diameter of the damaged area relative to enrgy(A) and number of shots(B). The colors correspond to the constant parameter value of a group os measurements, namely number of shots for (A) and pulse energy, in mJ, for (B).

(A) Damaged area relative to the energy of the shots.

(B) Damaged area relative to the number of shots done in a spot.

FIGURE A.3: Plots for the calculated damaged areas from the diameter values obtained relative to energy(A) and number of shots(B). The colors correspond to the constant parameter value of a group os measurements, namely number of shots for (A) and pulse energy in mJ for (B).

Energy [mJ]	Measurements of Depth [μm] (20 Pulses)
20.9	763.756
	794.875
	688.465
	666.238
	670.519
	690.681
27.9	1018.339
	1020.712
	926.910
	1005.622
35.0	895.629
	794.519
	930.912
	746.564
	929.988
41.6	1121.234
	1195.005
	1075.080
	1092.451
	1085.305
48.3	1323.808
	1460.174
	1415.796
	1280.236
	1237.091
	1328.382

TABLE A.4: Viable measurements obtained of the cavities. Due to irregularities of ablation, only the cavities that were easy to distinguish from the cork stopper were measured.
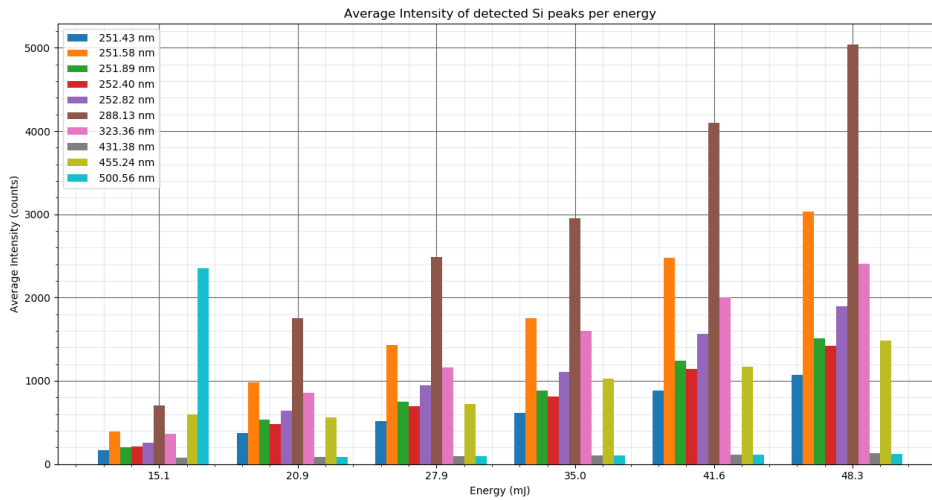
A.0.2 Energy Study

FIGURE A.4: Average intensity of Si lines detected on first shot of 80 nodes. These lines were present in at least 80% of the total spectra.
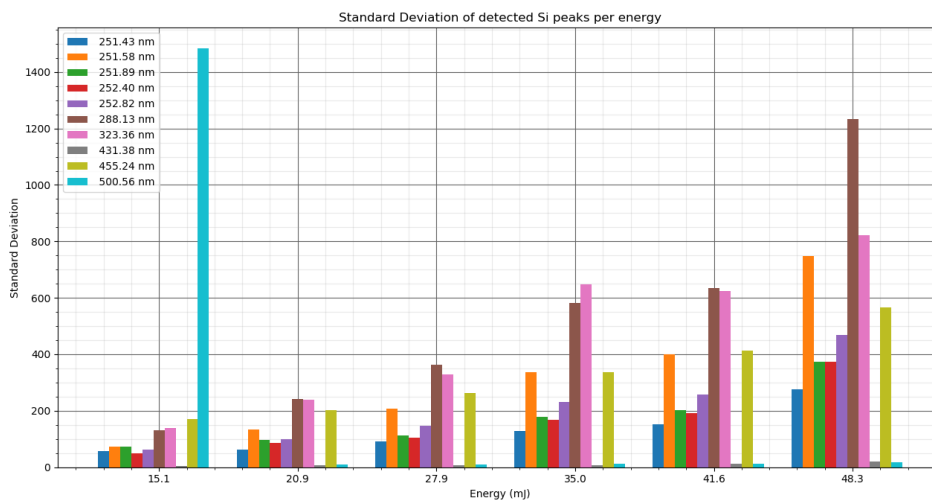

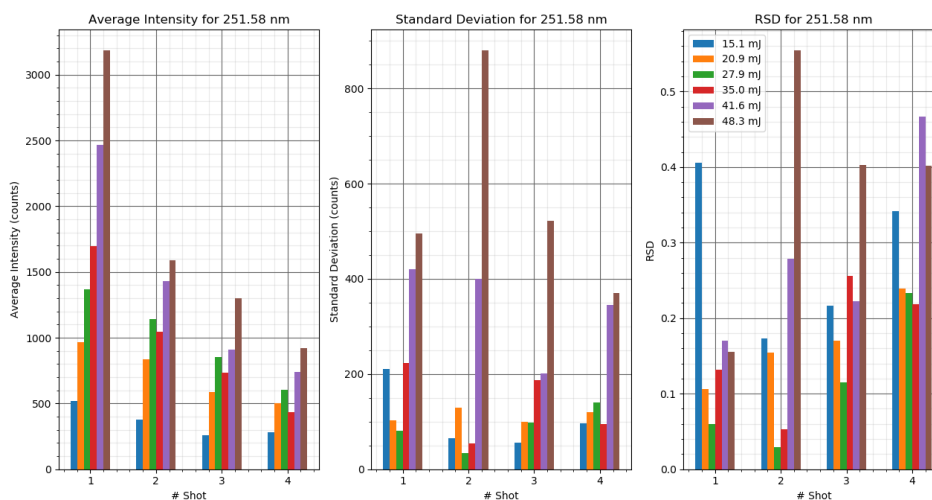FIGURE A.5: Standard deviation values obtained from the averages obtained and represented in A.4

FIGURE A.6: Average intensity, standard deviation and relative standard deviation of peak at 251.58 nm for the 4 shots made in each of the 3 nodes for each energy.

FIGURE A.7: Average intensity, standard deviation and relative standard deviation of peak at 251.89 nm for the 4 shots made in each of the 3 nodes for each energy.
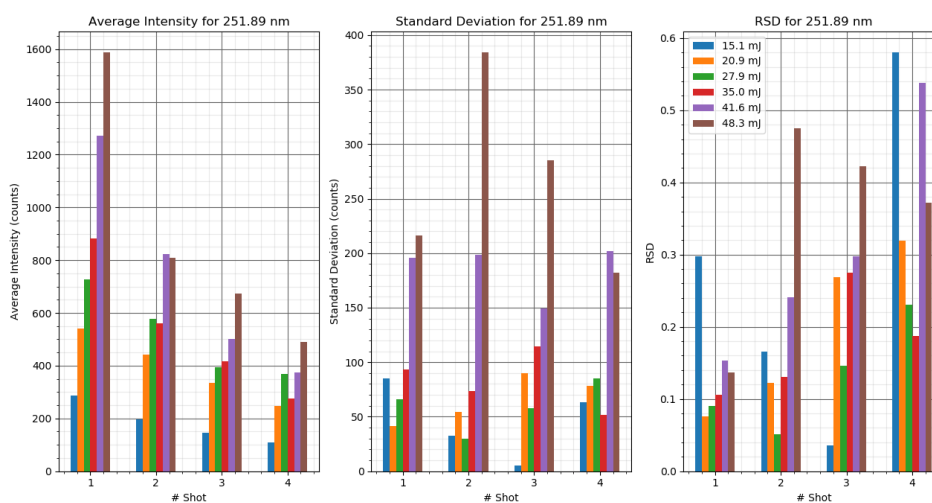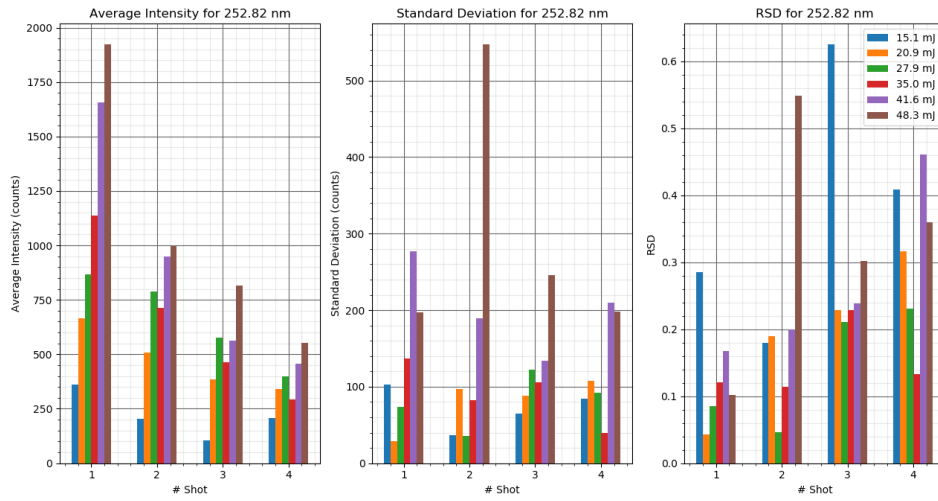
FIGURE A.8: Average intensity, standard deviation and relative standard deviation of peak at 252.82 nm for the 4 shots made in each of the 3 nodes for each energy.
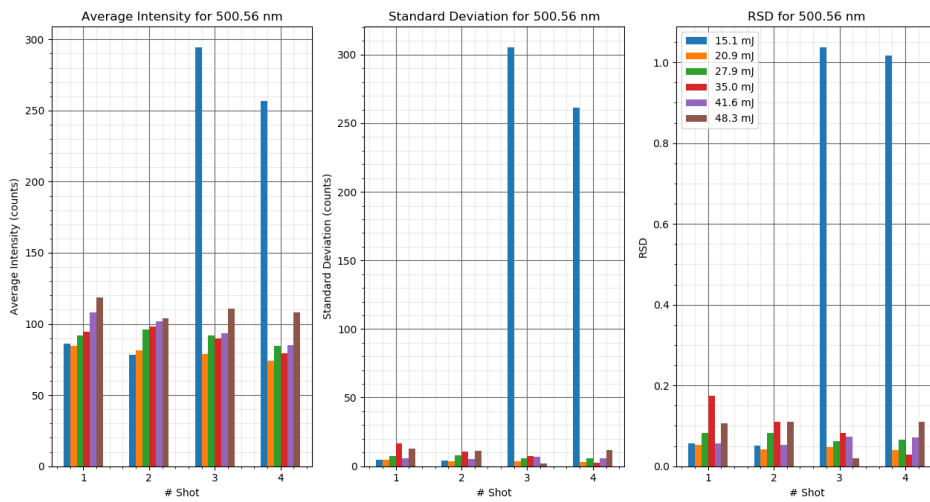

FIGURE A.9: Average intensity, standard deviation and relative standard deviation of peak at 500.26 nm for the 4 shots made in each of the 3 nodes for each energy.

A.0.3 Influence of Clean Shot

Shot #1		No Clean Shot - 4 x 20 Nodes			Clean Shot - 20 Nodes			Group
Lines (nm)		Average	Std	Rsd	Average	Std	Rsd	
	251,58	937,71	143,89	0,15	957,11	229,12	0,24	Group 1
	251,89	520,18	77,24	0,15	485,24	113,98	0,23	
	252,82	636,29	114,3	0,18	629,05	144,82	0,23	
	288,13	1681,32	281,5	0,17	1577,75	363,5	0,23	
	251,58	1030,21	110,17	0,11				Group 2
	251,89	551,35	88,67	0,16				
	252,82	658,61	68,61	0,10				
	288,13	1837,42	237,03	0,13				
	251,58	991,26	140,03	0,14				Group 3
	251,89	555	86,41	0,16				
	252,82	660,65	116,47	0,18				
	288,13	1794,51	211,74	0,12				
	251,58	967,24	128,79	0,13				Group 4
	251,89	518,19	121,14	0,23				
	252,82	622,43	94,15	0,15				
	288,13	1682,2	210,97	0,13				

(A) Calculations for shot number 1.

Shot #2		No Clean Shot - 4 x 20 Nodes			Clean Shot - 20 Nodes			Group
Lines (nm)		Average	Std	Rsd	Average	Std	Rsd	
	251,58	677,79	159,68	0,24	616,18	192,67	0,31	Group 1
	251,89	366,56	68,66	0,19	343,3	103,92	0,30	
	252,82	437,73	103,12	0,24	400,99	124,61	0,31	
	288,13	1233,2	231,44	0,19	1060,32	337,95	0,32	
	251,58	698,16	146,29	0,21				Group 2
	251,89	384,5	89,52	0,23				
	252,82	472,73	100,63	0,21				
	288,13	1273,71	231,57	0,18				
	251,58	694,37	155,8	0,22				Group 3
	251,89	378,57	100,41	0,27				
	252,82	461,33	117,58	0,25				
	288,13	1279,51	255,24	0,20				
	251,58	641,16	131,69	0,21				Group 4
	251,89	347,75	71,93	0,21				
	252,82	418,07	67,47	0,16				
	288,13	1123,39	176,65	0,16				

(B) Calculations for shot number 2.

FIGURE A.10: Average intensity, standard deviation and respectrive RSD values for peaks at 251.58, 251.89, 252.82 and 288.13 nm for four group of measurements of 20 shot points without clean shot and one group for 20 points with clean shot of 3.7 mJ made before the main shot
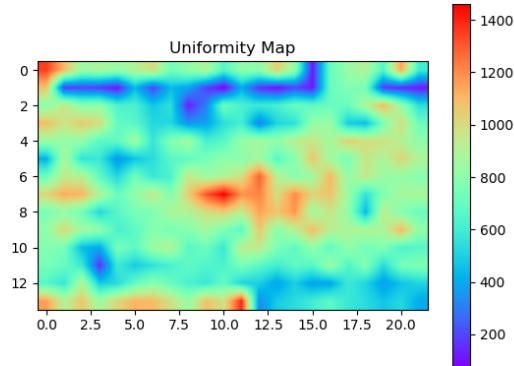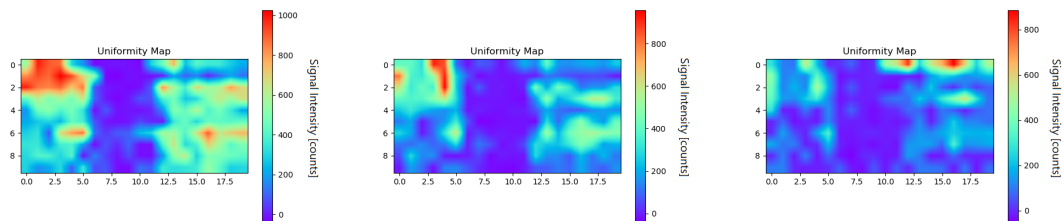
A.0.4   Uniformity Maps

FIGURE A.11: Uniformity map obtained at the 288.13 nm peak of the spectrum for a cork stopper with Si coating. The geometric shape expected was not possible to observe, probably due to the prior laser pulses shot the team did in a previous experiment. Similar pattern was seen when looking at uniformity maps at 251.58, 251.89 and 252.8.
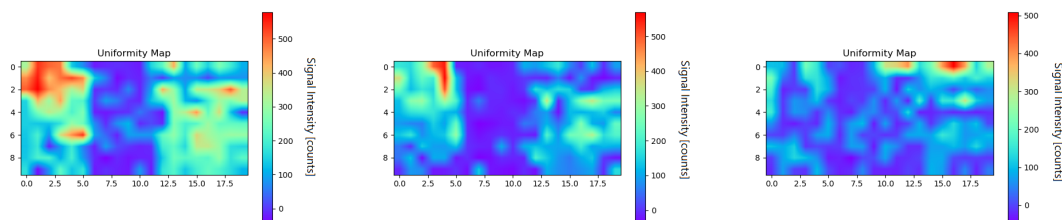

(A) Laser pulse shot number 1.

(B) Laser pulse shot number 3.

(C) Laser pulse shot number 6.

FIGURE A.12: Uniformity map obtained by looking at the 251.58 nm peak of the spectrum for a cork stopper with Si coating for shot 1 (A), 3 (B) and 6 (C). The same absence of signal detected with 288.13 nm can be seen.

(A) Laser pulse shot number 1.

(B) Laser pulse shot number 3.

(C) Laser pulse shot number 6.

FIGURE A.13: Uniformity map obtained by looking at the 251.89 nm peak of the spectrum for a cork stopper with Si coating for shot 1 (A), 3 (B) and 6 (C). The same absence of signal detected with 288.13 nm can be seen.

(A) Laser pulse shot number 1.

(B) Laser pulse shot number 3.
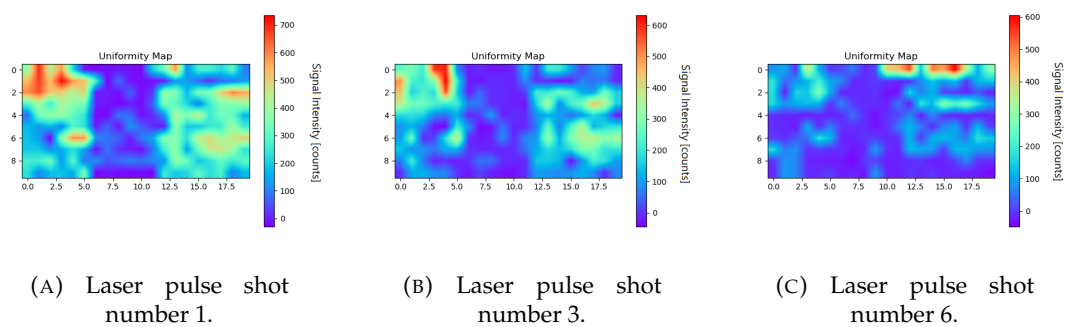
(C) Laser pulse shot number 6.

FIGURE A.14: Uniformity map obtained by looking at the 252.82 nm peak of the spectrum for a cork stopper with Si coating for shot 1 (A), 3 (B) and 6 (C). The same absence of signal detected with 288.13 nm can be seen.

A.0.5 Cork Mapping using PCA method
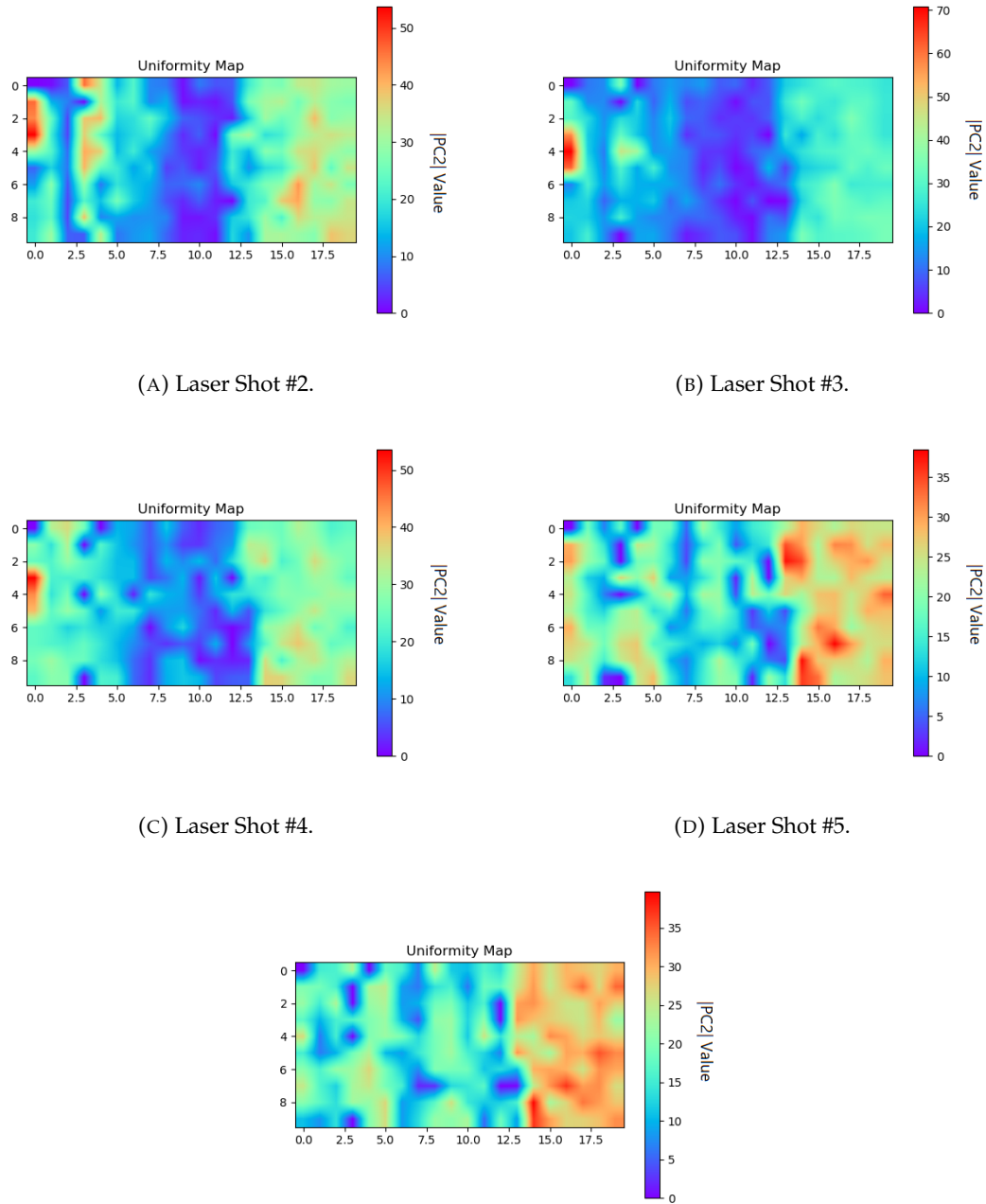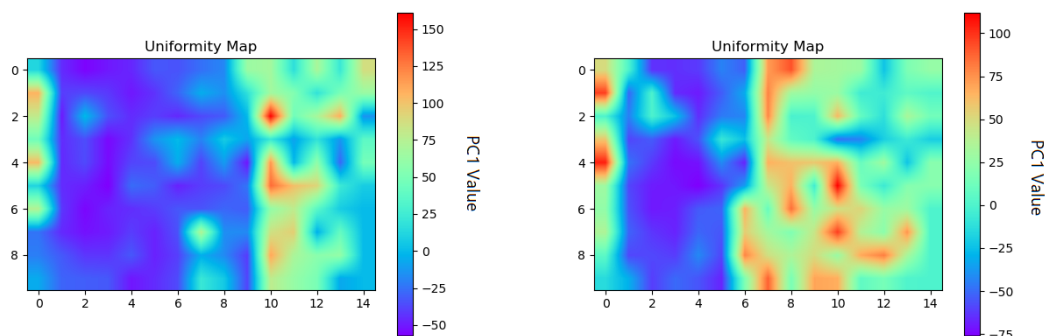
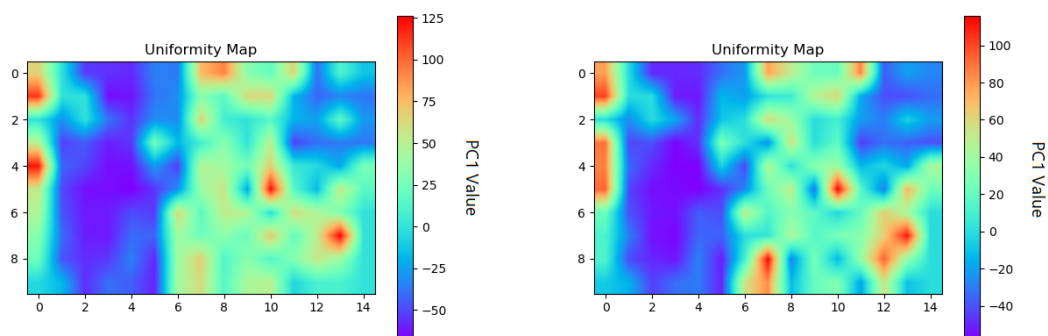### A.0.5.1 Mapping Si-coated Stopper

(A) Laser Shot #2.

(B) Laser Shot #3.

(C) Laser Shot #4.

(D) Laser Shot #5.

(E) Laser Shot Number 6.

FIGURE A.15: Uniformity map obtained using PCA method using norm of PC2 for all wavelength range of the data.

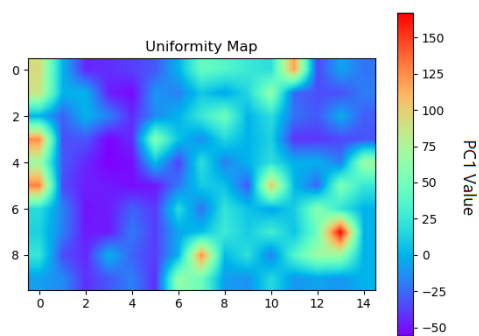### A.0.5.2 Mapping Paraffin-coated Stopper

(A) Laser Shot #1.

(B) Laser Shot #3.

(C) Laser Shot #4.

(D) Laser Shot #5.

(E) Laser Shot Number 6.

FIGURE A.16: Uniformity map obtained using PCA method in measurements made in Paraffin-coated cork stopper. Maps use PC1 values obtained from all wavelength range of the data.
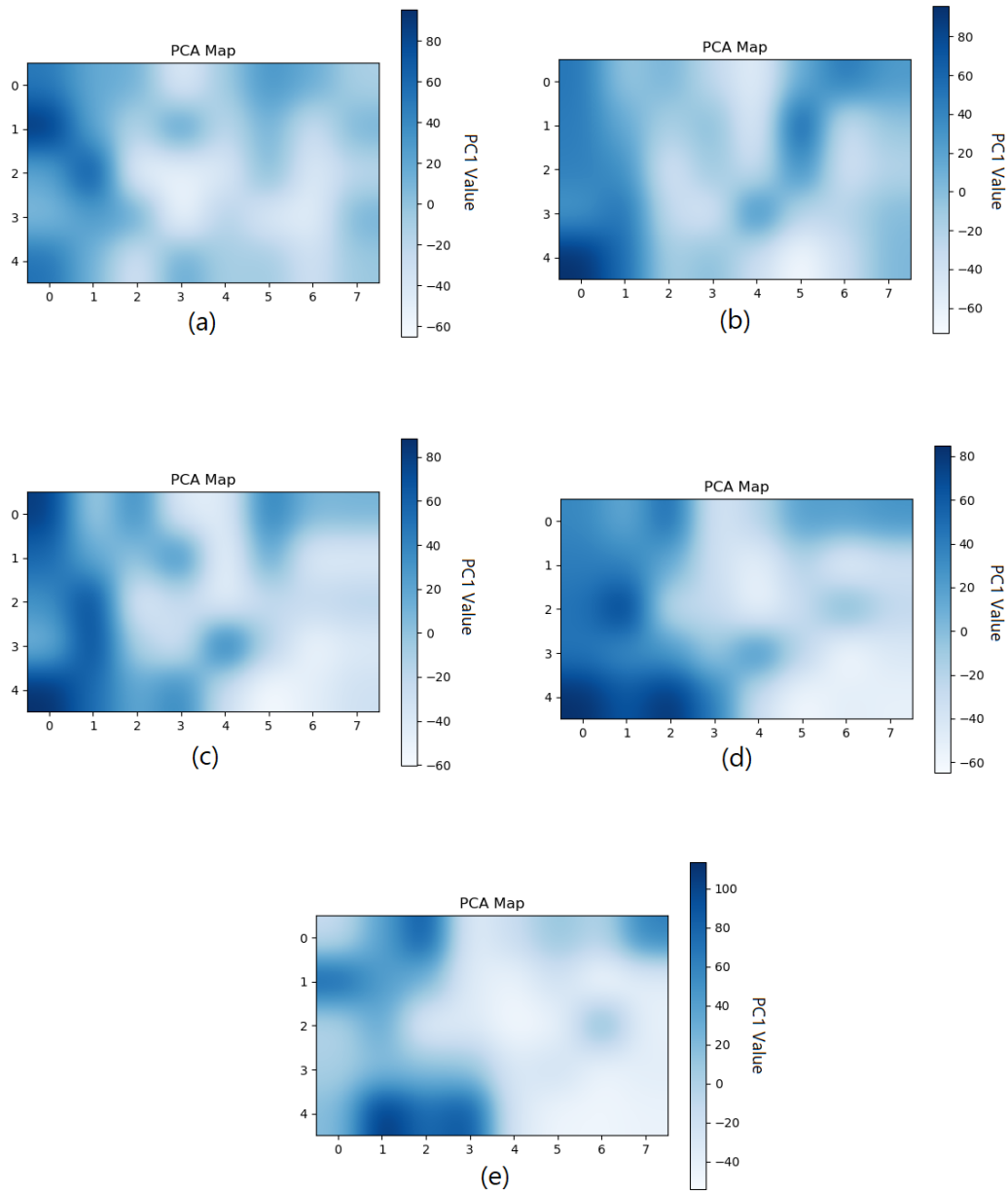
FIGURE A.17: Uniformity map obtained using shot number 1(a), 2(b), 3(c), 4(d) and 6(e) of all spots. As calculated for Figure 4.19, the percentage of correspondence of each map was of 70%, 60%, 70%, 75% and 77.5%, respectively.

Bibliography

[1] J. Pedarnig, J. Heitz, T. Stehrer, B. Praher, R. Viskup, K. Siraj, A. Moser, A. Vlad, M. Bodea, D. Bäuerle, N. H. Babu, and D. Cardwell, "Characterization of nano-composite oxide ceramics and monitoring of oxide thin film growth by laser-induced breakdown spectroscopy," *Spectrochimica Acta Part B*, vol. 63, no. 10, pp. 1117–1121, 2008. [Cited on pages 1 and 7.]

[2] D. A. Cremers and L. J. Radziemski, *Handbook of Laser-Induced Breakdown Spectroscopy: Second Edition*, Second, Ed., 2013. [Cited on pages xiii, 1, 2, 9, 10, 11, 12, 13, 14, 15, and 16.]

[3] E. Archbold, D. W.Harper, and T. P. Hughes, "Time-resolved spectroscopy of laser-generated microplasmas," *British Journal of Applied Physics*, vol. 15, pp. 1321–1326, 1964. [Cited on page 2.]

[4] C. C. Garcia, J. M. Vadillo, S. Palanco, J. Ruiz, and J. J. Laserna, "Comparative analysis of layered materials using laser-induced plasma spectrometry and laser-ionization time-of-flight mass spectrometry," *Spectrochimica Acta - Part B*, vol. 56, no. 6, pp. 923–931, 2001. [Cited on page 3.]

[5] H. Estupiñán, D. Y. Peña, R. Cabanzo, and E. Mejía-Ospino, "Analysis of the composition of titanium oxide coating by laser induced breakdown spectroscopy," *AIP Conference Proceedings*, vol. 992, no. April 2008, pp. 1213–1216, 2008. [Cited on page 4.]

[6] A. Dubey, G. Keyvan, R. Hsia, K. Saranteas, D. Brone, T. Misra, and F. J. Muzzio, "Analysis of pharmaceutical tablet coating uniformity by laser-induced breakdown spectroscopy (LIBS)," *Journal of Pharmaceutical Innovation*, vol. 6, no. 2, pp. 77–87, 2011. [Cited on page 4.]

[7] *Pharma Manufacturing - Pharma Laser*, (last access at October 2, 2020). [Online]. Available: https://scipython.com/book/chapter-8-scipy/examples/the-voigt-profile/ [Cited on page 5.]

[8] M. P. Mateo, V. Piñon, and G. Nicolas, "Vessel protective coating characterization by laser-induced plasma spectroscopy for quality control purposes," *Surface and Coatings Technology*, vol. 211, pp. 89–92, 2012. [Cited on page 5.]

[9] C. Basler, A. Brandenburg, K. Michalik, and D. Mory, "Comparison of laser pulse duration for the spatially resolved measurement of coating thickness with laser-induced breakdown spectroscopy," *Sensors (Basel, Switzerland)*, vol. 19, no. 19, 2019. [Cited on page 6.]

[10] J. H. In, C. K. K. S. H. Lee, and S. Jeong, "High precision prediction of thin film composition by LIBS," *2015 11th Conference on Lasers and Electro-Optics Pacific Rim, CLEO-PR 2015*, vol. 3, no. paper 27E2_1, 2016. [Cited on page 7.]

[11] J. Hermann, E. Axente, F. Pelascini, and V. Craciun, "Analysis of Multi-elemental Thin Films via Calibration-Free Laser-Induced Breakdown Spectroscopy," *Analytical Chemistry*, vol. 91, pp. 2544–2550, 2019. [Cited on page 8.]

[12] K. Miyamoto, *Plasma Physics for Controlled Fusion Second Edition*, 2015. [Cited on page 9.]

[13] G. D. Roston and F. S. Obaid, "Exact analytical formula for Voigt spectral line profile," *Journal of Quantitative Spectroscopy and Radiative Transfer*, vol. 94, no. 2, pp. 255–263, 2005. [Cited on page 12.]

[14] M. T. Meftah, H. Gossa, K. A. Touati, K. Chenini, and A. Naam, "Doppler broadening of spectral line shapes in relativistic plasmas," *Atoms*, vol. 6, no. 2, 2018. [Cited on page 13.]

[15] *Paschen-Back Effect*, (last access at November 7, 2020). [Online]. Available: http://hyperphysics.phy-astr.gsu.edu/hbase/quantum/paschen.html [Cited on page 14.]

[16] V. Oliveira and H. Pereira, "Cork and Cork Stoppers: Quality and Performance," *Winemaking - Stabilization, Aging Chemistry and Biochemistry [Working Title]*, 2020. [Cited on page 17.]

[17] *A Cortiça - O que é.*, (last access at November 11, 2020). [Online]. Available: https://www.amorim.com/a-cortica/o-que-e/ [Cited on page 17.]

[18] P. H. C. Eilers and H. F. M. Boelens, "Baseline Correction with Asymmetric Least Squares Smoothing," pp. 1–26, 2005. [Cited on pages 22 and 24.]

[19] P. H. Eilers, "Parametric Time Warping," *Analytical Chemistry*, vol. 76, no. 2, pp. 404–411, 2004. [Cited on pages 22 and 24.]

[20] *Python baseline correction library*, (last access at October 2, 2020). [Online]. Available: https://stackoverflow.com/questions/29156532/python-baseline-correction-library/29185844 [Cited on pages 22 and 24.]

[21] P. Nicolas Coca, *Removing Spikes from Raman Spectra with Anomaly Detection: Whitaker-Hayes algorithm in Python*, November 19, 2019 (last access at October 10, 2020). [Online]. Available: https://towardsdatascience.com/removing-spikes-from-raman-spectra-8a9fdda0ac22 [Cited on page 25.]

[22] *NIST Atomic Spectra Database*, (last access at November 7, 2020). [Online]. Available: https://www.nist.gov/pml/atomic-spectra-database [Cited on page 27.]

[23] S. Wold, K. Esbensen, and P. Geladi, "Principal component analysis," *Chemometrics and Intelligent Laboratory Systems*, vol. 2, pp. 37–52, 1987. [Cited on page 28.]

[24] J. Shlens, "A Tutorial on Principal Component Analysis," 2014. [Cited on page 29.]

[25] *Scikit learn - sklearn.decomposition.PCA*, (last access at October 15, 2020). [Online]. Available: https://scikit-learn.org/stable/modules/generated/sklearn.decomposition.PCA.html [Cited on page 29.]

[26] E. Tognoni and G. Cristoforetti, "Signal and noise in Laser Induced Breakdown Spectroscopy: An introductory review," *Optics and Laser Technology*, vol. 79, no. May, pp. 164–172, 2016. [Cited on page 31.]